NO_x Storage and Release Activity on Pd/BEA Passive NO_x Adsorber

A Thesis

Presented to

the Faculty of the Department of Chemical and Biomolecular Engineering

University of Houston

In Partial Fulfillment

of the Requirements for the Degree

Master of Science

in Chemical Engineering

by

Anh V. Vu

May 2017

Acknowledgements

My graduate journey toward my goal of achieving a PhD has been taking quite a few turns with mostly unfortunate events and had to be ended prematurely. Regardless of those difficult situations, the only person whom I know by heart that I can always turn to for academic advice and support is Dr. William Epling. Despite many kinds of burdens he has to carry, his inspirational and optimistic attitude in the most disciplined manner still manifests in all of our meetings and encounters. I may not even be his average-quality student due to my background and personality, but throughout 4 years of his guidance I can see myself growing meeting by meeting, email by email, in terms of critical thinking on resolving challenging engineering and scientific problems. Of all the lessons he has taught me, I find this one the most meaningful: you are the one and only teacher of your life; no matter what life throws at you, it will be either you get up by yourself or you will slide downhill forever; no one will ever have enough concern for your own endeavor and life problems but yourself. So thank you, Dr. Epling.

Along this journey I have also had a chance to converse at various levels with a lot of talented individuals in the department of Chemical and Biomolecular Engineering at the University of Houston. I would like to especially express my gratitude to Mr. Yasser Jangjou, a colleague in my graduate career. And a great friend, if not the best. He is my mental support, my motivation, my life-issue trash can where no one else cares enough to be. Graduate life is tough. That is a well-established and evident fact. But I have never been through a frustrating day in my graduate life with Yasser by my side. He has taught me to be strong and independent, in my very own way. He has sprung me up from valleys of depressions. Thank you, Yassi.

Research demands financial investment; that is for sure. I could not be thankful enough for the financial support from Cummins Inc. I felt very apologetic about my unsuccessfully producing sufficient quality result, but I know at least I am grateful for all the research opportunities that have been given by Cummins Inc. The only regret I have is that I have never had a chance to meet the people behind my projects in person so that I could thank them for their involvement and investment. Other than Cummins Inc., I would like to express my gratitude to Dr. Hai-ying Chen from Johnson Matthey, PLC, for his generous inputs on the making of Pd/BEA passive NOx adsorber.

Early in my graduate career, I was trained by Dr. Di Wang and Dr. Tayebeh Hamzehlouyan. Obviously without their efforts, I would not have been even able to accomplish this study due to the lack of basic research skills. In terms of research, I feel the need to also acknowledge fruitful discussions with them both, Dr. Justin Dodson, Dr. Chaitanya Sampara, Dr. Monique Wilburn, and Dr. Melanie Hazlett, briefly or deeply. Certainly, their inputs have already manifested in every word in this thesis. Along this path, I also need to mention Dr. Munish Sharma, Dr. Syed Ali Gardezi, Francesco Piubello, Dr. Khalid Azzam, Dr. Vecon Easterling, Peter (from Denmark), Quan Do, Dr. Hung Tran, Kyle Karinshak, Vikash Patel, Paige Atchison, Mohammad Safari, Dr. Sung-bong Kang, Courtney Littlejohn, Kevin Gu, Yongjie Ren, and Gary Gildert. They have completed my graduate life.

I would also like to thank Dr. Jacinta Conrad, Dr. Vincent Donnelly, Dr. Gila Stein, Dr. William Epling, Dr. James Richardson, Dr. Jeffrey Rimer, Dr. Lars Grabow, Dr. Vemuri Balakoitaiah, Dr. Edwin Carrasquillo, and Drs. Kate Olafson, Melanie Hazlett, Patrick Cirino, Megan Robertson, Demetre Economou, Michael Nikolaou,

Katerina Kourentzi, for their academic teaching and lectures. The knowledge I have gained from them is invaluable. And as part of the department of Chemical and Biomolecular Engineering, I would like to include the staffs who have made consistent efforts to maintain the administrative aspects, especially Ms. Yolanda Thomas, Ms. Nicolette Solano, and Ms. My Lieu (previous staff).

And the most important of all, the backbone of my accomplishments: my mom, my dad, and my brother.

NO_x Storage and Release Activity on Pd/BEA Passive NO_x Adsorber

An Abstract

of a

Thesis

Presented to

the Faculty of the Department of Chemical and Biomolecular Engineering

University of Houston

In Partial Fulfillment

of the Requirements for the Degree

Master of Science

in Chemical Engineering

by

Anh V. Vu

May 2017

Abstract

Increasingly stringent vehicular emission regulation on NO_x demands a better strategy to further mitigate tailpipe NO_x exhaust. In terms of NO_x reduction strategy, both current state-of-the-art technologies, selective catalytic reduction (SCR) and NO_x storage and reduction (NSR), have shown optimal performance in warm conditions but are not fully functional at temperature below 200°C, commonly regarded cold-start condition. Thus, in order to mitigate NO_x cold-start emission, the passive NO_x adsorber (PNA) has been introduced. Among the potential PNAs, Pd/BEA stands out due to its promising NO_x storage capacity and well-controlled thermal desorption performance. In this Masters thesis, NO_x adsorption and desorption on Pd/BEA was studied using temperature-programmed desorption method. It was shown that CO improved NO_x storage and induced NO_x release to higher temperature on Pd/BEA where the chemical state of Pd is key. The desorption kinetics of NO_x on Pd/BEA was also studied in an attempt to resolve the effect of heating rate on the controlled release of NO_x.

Table of Contents

List of Figures

List of Tables

Nomenclature

b	Slope of compensation effect relation [mol·K·J^{-1}]
β	Heating rate [K·min^{-1}]
c	Intercept of compensation effect relation [1]
ΔE_d	Activation energy of desorption relative to $E_{d,0}$ [J·mol^{-1}K^{-1}]
E_d	Activation energy of desorption [J·mol^{-1}K^{-1}]
$E_{d,0}$	Activation energy of desorption at $\theta = 0$ [J·mol^{-1}K^{-1}]
$g'(\theta)$	First derivative of surface coverage function [1]
KM	Kubelka-Munk unit [arbitrary]
n	Desorption order [1]
R	Universal gas constant [J·mol^{-1}K^{-1}]
R_∞	Transmittance unit [1]
r_i	Desorption rate of peak i [s^{-1}]
T	Temperature variable [K]
T_c	Isokinetic temperature [K]
T_i	Temperature variable for peak i [K]
T_p	Peak temperature location [K]
θ	Surface coverage [1]
θ_i	Surface coverage of peak i [1]
θ_0	Initial surface coverage [1]
$\theta_{0,i}$	Initial surface coverage of peak i [1]
ν_n	Frequency factor associated to desorption order n [s^{-1}]
ν_2	Frequency factor associated to 2nd order desorption [s^{-1}]
W	Interaction energy among lateral adsorbates [J·mol^{-1}K^{-1}]
$W_{1/2}$	Half-width of a desorption peak [K]
$W_{3/4}$	Three-quarter-width of a desorption peak [K]

Chapter 1 – Introduction and Background

Since the enactment of the Air Pollution Control Act of 1955, significant research activity has been directed at mitigating air pollution from both stationary and mobile sources. It was not until the Clean Air Act of 1970 that control over vehicular emissions was lawfully enforced and promulgated, and further emission standards became effective with the 1990 Amendments. Among the regulated pollutants, nitrogen oxides (NO_x) abatement has posed a significant challenge as its lawful emission level was dropped by more than 20 times with 2010 standards, compared to approximately 10 times in the case of hydrocarbons (HCs) and particulate matter (PM), as shown in Table 1. Despite stringent emission regulations, NO_x reduction has been a success story in diesel engines thanks to selective catalytic reduction (SCR) and NO_x storage and reduction (NSR) technologies. SCR involves selective decomposition of nitrogen oxides in an oxidizing environment by a reducing agent, most notably ammonia or hydrocarbons from fuel; whereas NSR stores NO_x on the catalysts first and then non-selectively reduces the trapped NO_x typically under fuel-rich gas [1]. Both have shown major improvements in reduction efficiencies in recent years with broader active temperature windows and more cost-effective catalysts. However, their performance is constrained at low temperatures, and because of these limitations, most NO_x will slip through the aftertreatment system when the catalyst temperatures are below approximately 200 °C. Such low temperatures are associated with cold-start emissions and can constitute a major portion of the total NO_x emitted during a drive cycle.

Table 1 - Emission regulations for U.S. trucks [2]

	1994	**1998**	**2003**	**2007**	**2009**	**2010**
HC	1.3	1.3	0.5	0.5	0.14	0.14
NO_x	5	4	2	2	0.2	0.2
PM	0.1	0.1	0.1	0.01	0.01	0.01

1.1 Cold-start emission

The cold-start period generally refers to the first few minutes of engine operation after a long uninterrupted soak, such as an overnight idle. Cold-start can also refer to an engine start when both the engine and the catalytic converter are within 10°C of the ambient temperature (EPA 1993). Such low temperatures typically render the aftertreatment system inactive or at low efficiency, with the majority of diesel exhaust slipping through unconverted, as shown in Figure 1. Among the exhaust constituents, oxides of nitrogen are of serious concern, especially for diesel engines, which typically emit more NO_x than spark-ignited engines equipped with a three-way catalyst. Many strategies have been proposed to reduce cold-start emissions that range from controlled heating of either the engines or the aftertreatment system to improving the design of catalytic converter [3,4]. Part of recent research efforts has also been directed at improving pre-existing catalysts. In terms of NO_x abatement, both of the aforementioned technologies have been considered for increasing activity at low temperatures, especially in SCR catalysts.

1.2 Selective catalytic reduction

SCR is a catalytic process that converts NO_x to nitrogen and water using a reducing agent, commonly NH_3 or HCs. First developed for NO_x abatement in stationary sources in Japan in the 1970s, SCR has become the most effective and globally applied de-NO_x

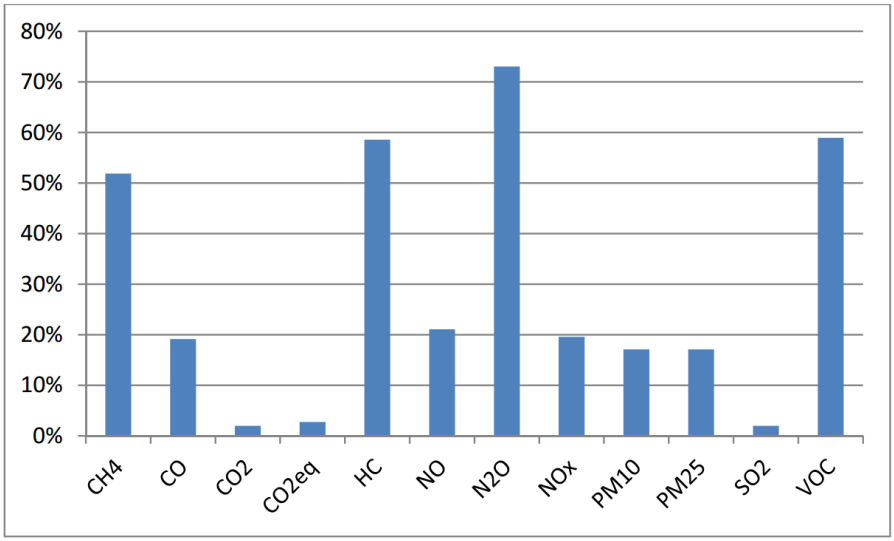

Figure 1 - Percentage of running and starting emissions attributable to starts (MOVES output). Travis County, Texas, July 2010 weekday, Light-Duty Vehicles only [5]

technology [6]. Among the first catalysts considered for the SCR processes, supported vanadia has been the most extensively studied. A study by Lietti et al. shows that NO_x conversion starts at around 150°C for V_2O_5/TiO_2 (promoted with either WO_3 or MoO_3) and reaches maximal value from 300-450°C [7,8]. However, this active temperature window is still narrow compared to the temperature range in diesel exhaust and a large portion of NO_x remains unreacted at temperatures lower than 200°C. Among the many transitional metal oxide candidates that have been then proposed to improve de-NO_x activity at low temperature, MnO_x-based catalysts stand out as the most promising solution as they can achieve more than 90% NO_x conversion at temperatures as low as 50°C. The performances of many variations of MnO_x catalysts are summarized in Table 2. However, activity at high temperatures, above 300°C, is not sufficient, and the testing conditions were water-free, which does not resemble realistic diesel exhaust conditions [8]. As an example of an attempt to develop a water-tolerant SCR catalyst, An et al. proposed Pt/fluorinated carbon with high NO_x reduction activity between 170-

275°C in the presence of 4% H_2O [9]. However, this limited temperature window of activity does not meet the wide temperature range in diesel exhaust. Despite much research effort, significant drawbacks of metal oxides catalysts in terms of providing persistent activity in a wide temperature range still remain.

Table 2 - Research results on three kinds of Mn-based catalysts in literatures (excerpt from ref. [8]).

Catalysts	**Reaction conditions**	**Highest NO_x conversion/N_2 selectivity (T range)**
Non-supported MnO_x		
MnO_x	0.05%NH_3, 0.05%NO, 5%O_2, 50,000 h^{-1}	100%/>82% (100–150°C)
Manganese ore	0.045%NH_3, 0.04%NO, 3%O_2, 20,000 h^{-1}	100% (150–250°C)
Mn-based composite oxides		
MnO_x-CuO	0.05%NH_3, 0.05%NO, 5%O_2, 30 000 h^{-1}	100%(50–200°C)
MnO_x-FeO_x	0.1%NH_3, 0.1%NO, 2%O_2, 15 000 h^{-1}	100% (120–180°C)
MnO_x-FeO_x-TiO_2	0.05%NH_3, 0.05%NO, 5%O_2, 50,000 h^{-1}	100%/>90% (200–300°C)
MnO_x-CeO_2	0.1%NH_3, 0.1%NO, 2%O_2, 42,000 h^{-1}	100% (120–150°C)
MnO_x-SnO_2	0.05%NH_3, 0.05%NO, 3%O_2	100% (120–200°C)
Mn supported catalysts		
MnO_x/Al_2O_3	0.055%NH_3, 0.055%NO, 2%O_2, 58,000 h^{-1}	95%/>65%(150–250°C)
MnO_x/TiO_2	0.1%NH_3, 0.1%NO, 3%O_2, 40,000 h^{-1}	100% (120–200°C)
MnO_x-CeO_2-Nb_2O_5/cordierite	0.2%NH_3, 0.1%NO, 10%O_2, 52,000 h^{-1}	80%/96% (200°C)
MnO_x/AC/C	0.055%NH_3, 0.05%NO, 3%O_2, 10,610 h^{-1}	95% (250°C)

Beside metal oxides, zeolite-based catalysts also emerged as another promising candidate for SCR processes. Noble metal-zeolites drew the majority of research

attention early. They have high NO_x reduction performance mostly at elevated temperature, but display narrow temperature windows and are susceptible to H_2O inhibition. Reactivity is severely hindered in the presence of water or on hydrothermally aged catalysts. Also, but of lesser research interest, are Ag-zeolite catalysts. Studies have shown that Ag-zeolites have improved temperature activity range and high resistance to water and even SO2, but their stability is limited due to the formation of AgO. Much more promising are the transition metal-zeolites, especially Fe-, and Cu-zeolites [10]. Fe-zeolites in general can maintain a relatively high NO_x conversion from around 300-550°C in the presence of water, though reactivity was very limited (<20%) below 200°C [11–14]. The limited activity at low temperature is improved with the substitution of Cu exchanged into small-pore zeolites, especially Cu-SSZ-13, which shows excellent NO_x conversion at temperatures as low as 200°C. [6,14]. The zeolite-based catalysts clearly surpass metal oxides in terms of low-temperature activity and wide temperature window. However, with the increasing challenge of meeting the current NO_x emission levels, the NO_x slipping through the tailpipe when the exhaust temperature is below 200°C still remains a great concern.

1.3 NO_x storage and reduction

Another technology that has also received research attention is NO_x storage and reduction, also known as the lean NO_x trap (LNT). Contrary to SCR, NSR first stores NO_x under lean conditions and then reduces the stored NO_x with fuel rich gas. However, the active temperature window for NSR catalysts is narrower, typically falling into the 250-450°C range [1]. The LNT system is often combined with SCR catalysts to improve overall activity, by using any over-reduced NO_x in the form of

NH3. Zheng et al. have studied a new dual-layer LNT-SCR design, which successfully achieved up to 80% NO_x conversion at around 200°C at 70k h^{-1} GHSV under lean conditions. It is noted also in terms of operation, streams of hydrocarbons, C3H8 in this study, were pulsed at high-frequency, approximately 4 pulses every 25 seconds, during rich cycles. Figure 2 shows that the light-off temperature for NO_x conversion is enhanced quite significantly by three factors: reducing lean/rich cycle time from 30/5s to 6/1s, increasing PGM loading, and adding an SCR layer [15]. Though inferior to SCR technology in terms of low temperature deNO_x activity, this improvement in NSR catalysts is particularly useful for smaller diesel passenger cars where NSR is more prevalent.

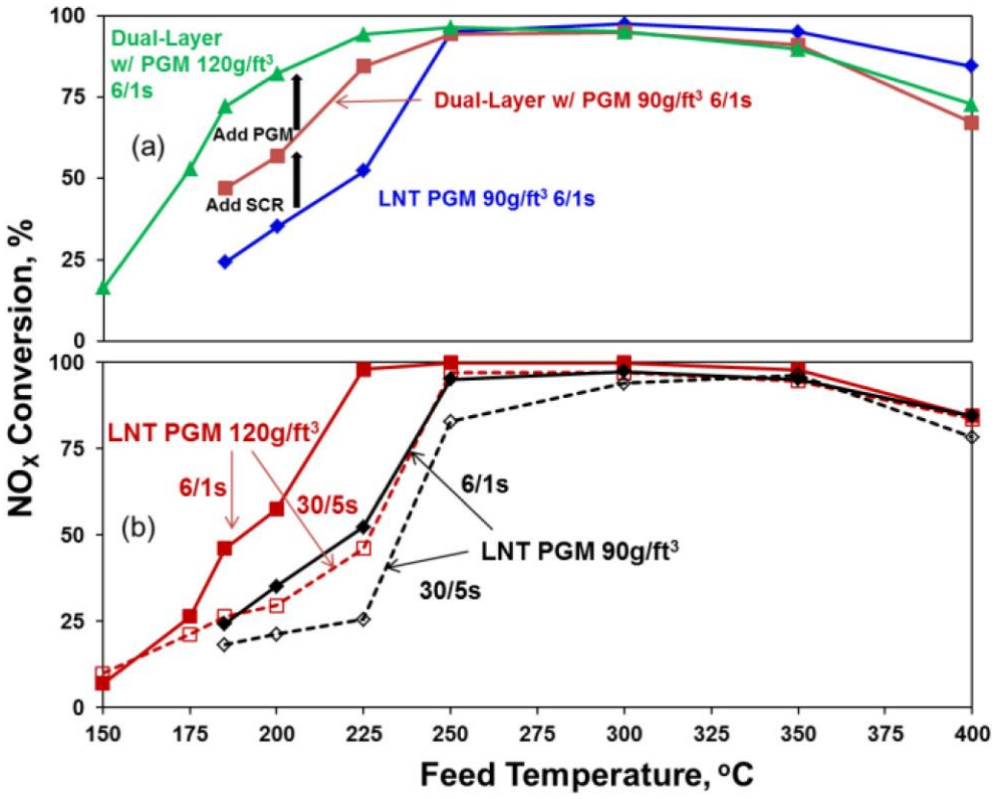

Figure 2 - Cycle-averaged NO_x as a function of feed temperature by (a) LNT, dual-layer catalysts with different PGM loading under the same fast cycling and (b) LNT alone with varied PGM loading and varied cycle times.

1.4 Passive NO_x adsorbers

The concept of NSR has provided a well-established groundwork for NO_x adsorption. In fact, one of the most recent strategies to mitigate cold-start emissions involves storing NO_x at low temperature then releasing it for downstream reduction when the exhaust temperature surpasses 200 °C. Passive NO_x adsorbers have been designed and developed to do just this [16]. For passive NO_x adsorber systems, the gas phase is assumed to be always fuel lean and NO_x is to be reduced on downstream catalytic components. Studies have shown promising passive NO_x adsorbers ranging from mixtures of transition metal oxides to metal-containing zeolites [17–20]. Cole proposed an incorporation of a NO_x adsorber catalyst immediately upstream of the three-way catalyst, whose combined NO_x reduction performance is shown in Figure 3. According to Cole, the NO_x sorbent catalyst can be composed of chromium oxide, nickel oxide, copper oxide, manganese oxide, iron oxide, zinc oxide, molybdenum oxide, cobalt oxide, or their mixtures, supported on alumina beads. The material screening criterion was as simple as establishing NO_x adsorbing characteristics, with the desired NO_x desorption temperature being at least 180°C. The author also showed the superior NO_x uptake capacity of chromium oxide over other metal oxides, as shown in Figure 4 [17].

Others have incorporated precious metals on alumina to store and release NO_x under oxidizing conditions [21,22]. Ji et al. studied Pt/Al_2O_3 as well as $Pt/La/Al_2O_3$ as potential passive NO_x adsorbers [22]. They found that the addition of La to Pt/Al_2O_3 improved NO_x storage at low temperature by enhancing nitrate formation. However, this limited NO_x desorption below 250 °C, in other words the nitrates may be

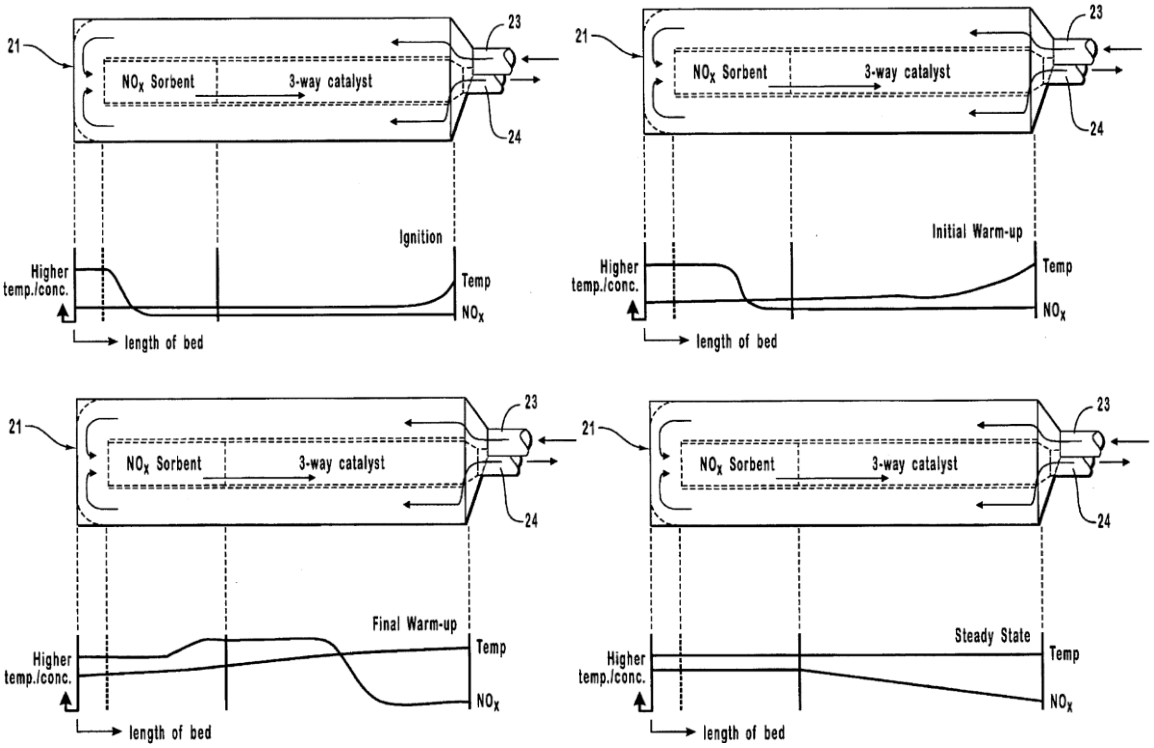

Figure 3 - Schematic diagrams illustrating the sequence of temperature and NO_x concentration trends that occur in the sorbent and catalyst bed during a complete cycle as operated in an automotive application [17].

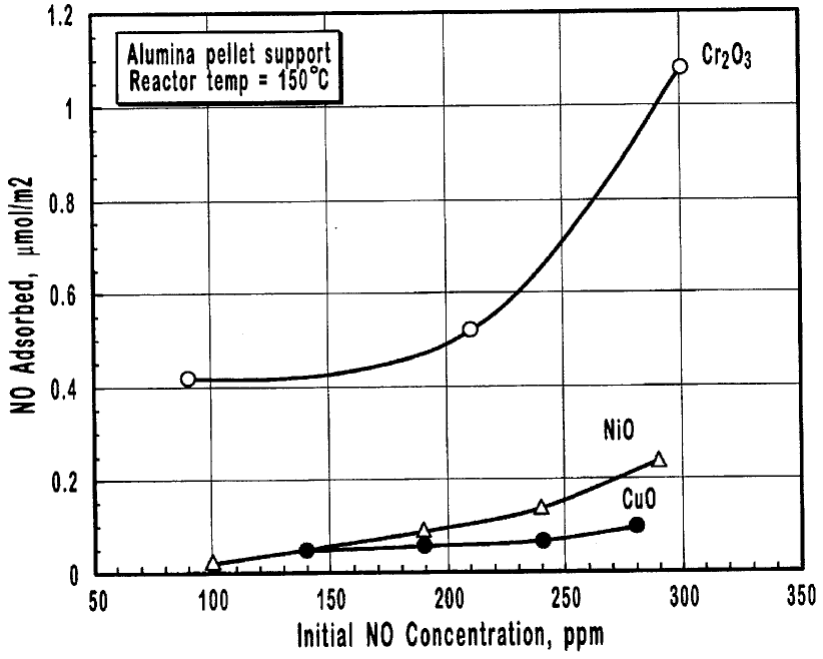

Figure 4 - Experimental results revealing adsorption isotherm capabilities of several sorbent materials [17].

too stable to be released in a more ideal temperature range. Ceria-based catalysts also appear to be potential passive NO_x adsorbers due to their low-temperature NO_x activity and applications in NSR and SCR [23–25]. Ryou et al. found that hydrothermally aged Pd/CeO_2 could retain NO_x until after 200°C, as shown in Figure 5 [23]. In Figure 6, the study also showed that the addition of Pt amplified the higher temperature β peak, which represented the NO and NO_2 decomposed from nitrate species. Furthermore, longer exposure of NO_x (500s – 3h, shown in Figure 7) promotes the formation of the lower temperature NO_x desorption peak, which starts below 150°C. Ceria also shows promising results in terms of boosting NO_x storage capacity when doped into a zirconia-based catalyst [24]. NO_x storage and release on ceria-based catalysts doped with Pd, Pt, and rare earth elements was also investigated, and Pd/CeO_2 loaded with 20 mol% Pr had significant NO_x storage at 120°C and NO_x release below 350°C [25]. Moreover, hydrothermal aging significantly affected NO_x storage capacity in all tested samples while improving NO_x desorption efficiency regarding NO_x released below 350°C.

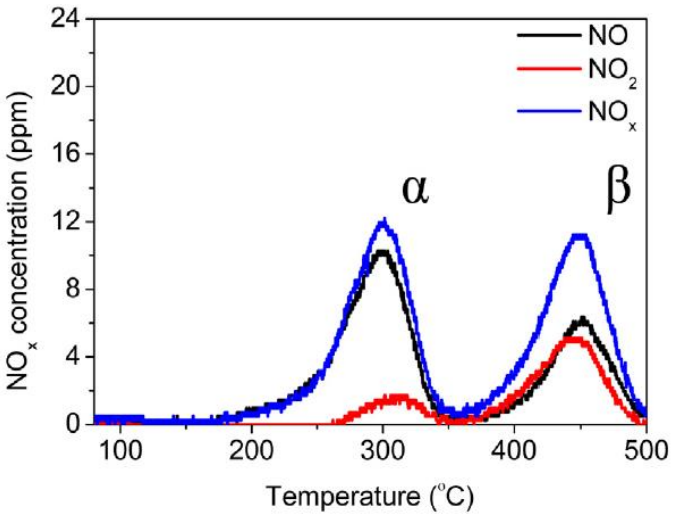

Figure 5 - NO, NO_2, and NO_x desorption curves of HTA Pd/CeO_2catalyst. (NO adsorption temperature: 80°C, ramping rate: 10°C/min). [23]

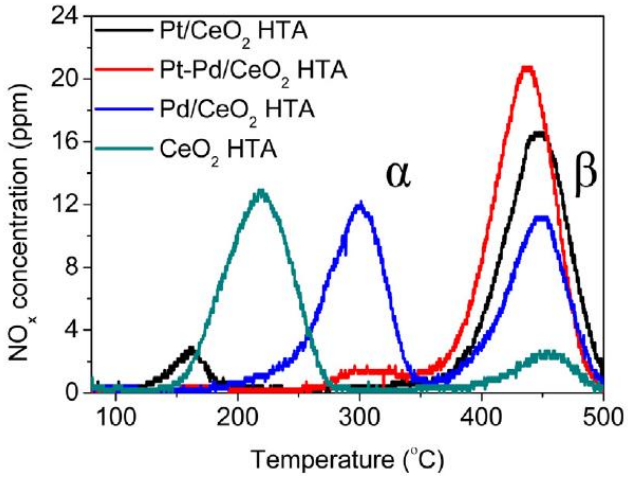

Figure 6 - NO_x desorption curve of HTA CeO_2 support and Pt, Pt-Pd, and Pd supported on CeO_2 catalysts. [23]

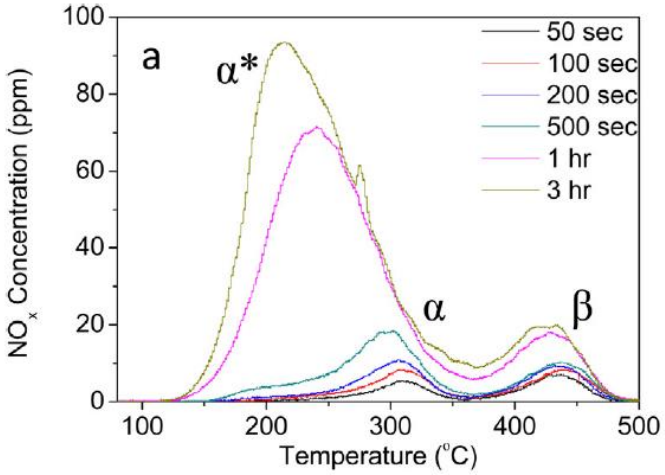

Figure 7 - NO_x desorption curves of HTA Pd/CeO_2 with the NO adsorption time for 50, 100, 200, 500 s, 1 and 3 h. [23]

In terms of zeolite based adsorbers, Chen et al. compared Pd catalysts supported on CeO_2 and MFI, CHA, and BEA zeolites [20]. All four catalysts showed considerable NO_x storage and desorption efficiencies. Chen et al. also investigated the effect of sulfur NO_x storage capacity on those catalysts and concluded that zeolite-supported catalysts sustained sulphation much better than CeO_2-supported. However, Pd/BEA appeared better than the other catalysts in terms of NO_x storage at 100 °C or lower and NO_x release above 200°C.

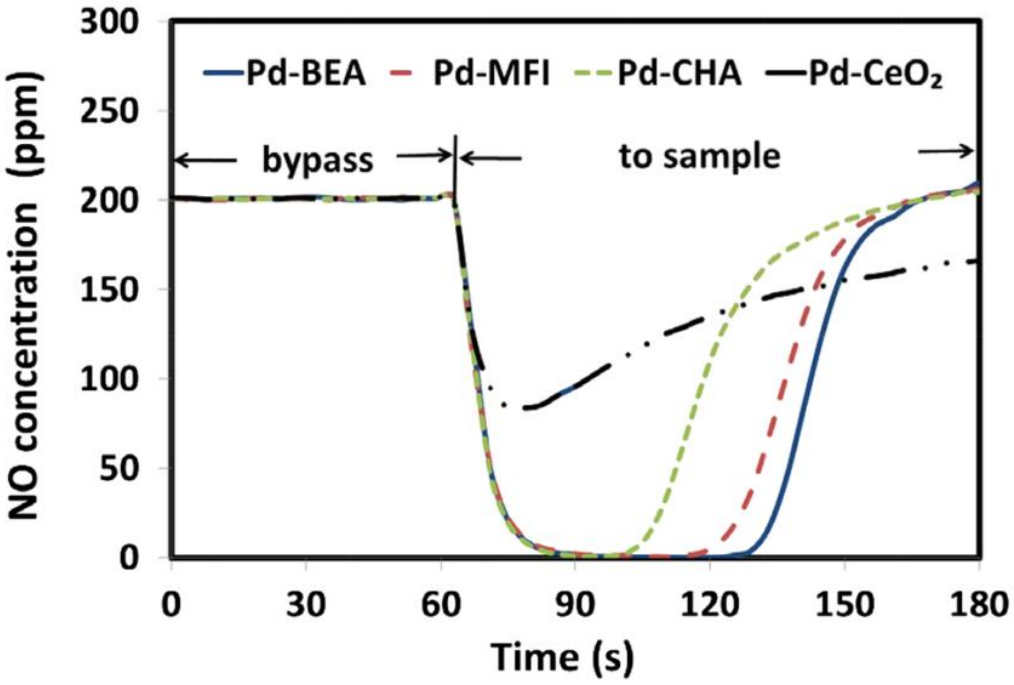

Figure 8 - NO adsorption at 100°C on different 1 wt.% Pd samples in a gas mixture containing 200 ppm NO, 200 ppm CO, 50 ppm C10H22, 12 % O_2,5 % CO_2,5%H_2O, and balanced with nitrogen [20]

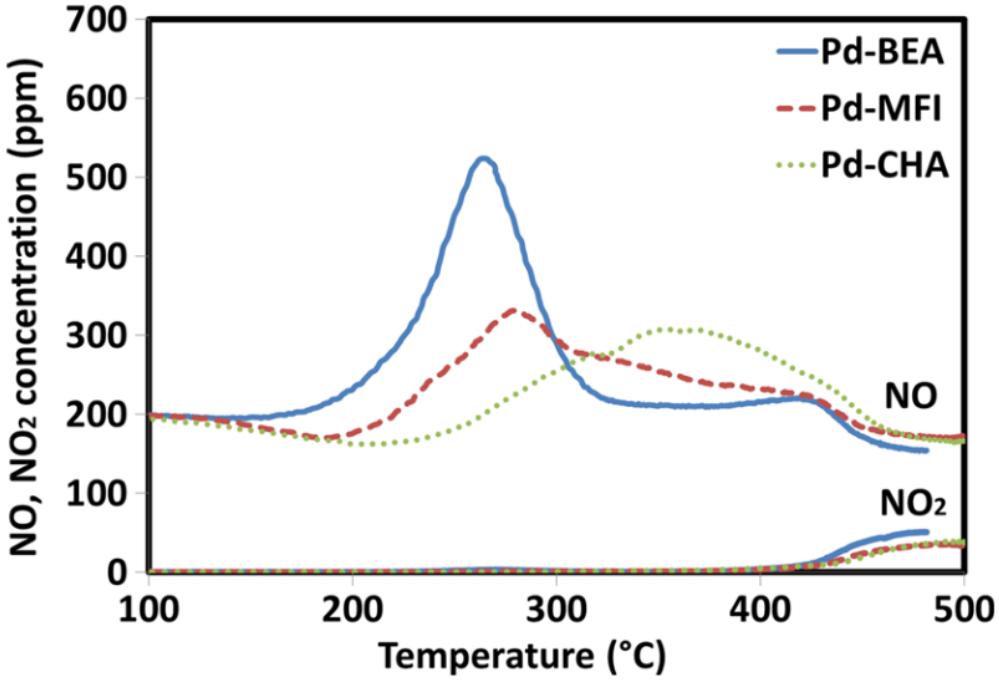

Figure 9 - NO and NO_2 release profiles for different Pd–zeolite samples after adsorption experiments at 100°C. Feed gas: 200 ppm NO, 200 ppm CO, 50 ppm $C_{10}H_{22}$, 12% O_2, 5% CO_2, 5% H_2O, and balanced with nitrogen [20]

1.5 Research objectives and thesis outline

State-of-the-art aftertreatment catalysts are approaching their optimal performance possible in terms of reactivity, selectivity, stability, and affordability. Thus, the low temperature condition where commercial catalytic converters have poor performance is crucial in addressing the increasingly stringent emission regulations. Cold-start emissions are well acknowledged and documented in recent decades. Research efforts have often focused on improving pre-existing catalysts. In terms of NO_x abatement, selective catalytic reduction (by ammonia or hydrocarbons) and NO_x storage and reduction are currently the most promising technologies. However, their activity at low temperature remains insufficient despite recent improvements.

Parallel to the path toward achieving a better low temperature SCR and/or NSR catalyst is the evolution of passive NO_x adsorbers (PNAs) which ideally trap NO_x in diesel exhaust at low temperature and then release it for downstream reduction when the exhaust temperature surpasses 200°C. PNA has gone through extensive catalyst screening and selected candidates have shown very promising results in terms of NO_x storage capacity at low temperature and their thermally controlled NO_x desorption efficiency. Among the top candidates is Pd/BEA. Though the performance of Pd/BEA has been shown superior to that of other PNA catalysts, the fundamental understanding of its performance is lacking. Therefore, in this thesis, I studied the NO_x adsorption behavior of Pd/BEA under relevant conditions and attempted to characterize at the surface level the possible adsorption events. The effect of CO on activity of Pd/BEA was also studied.

This thesis will be outlined as followed. In chapter 2, the overall experimental methodology will be discussed. Chapter 3 will discuss the effect of CO on Pd/BEA passive NO_x adsorbers. Chapter 4 summarizes the effect of SO_2 on Pd/BEA by evaluating NO_x activity under SO_2 flow. Chapter 5 will attempt to explore the kinetics of NO_x desorption on Pd/BEA in O_2, CO, and H_2O flows. Chapter 6 will summarize all the important points in this thesis and provide insights into the future directions.

Chapter 2 – Experimental Methods

Two reactor systems were used in this thesis. The bench scale reactor system with powder catalyst sample was used to conduct temperature-programmed desorption (TPD) experiments. An in-situ diffuse reflectance infrared Fourier transform spectroscopy (DRIFTS) reactor system was used for surface species identification under reaction conditions. The catalyst used in thesis was 1wt.% Pd/BEA (SAR = 25) in powder form. Further details about the two reactor systems, and catalyst preparation are presented in this chapter.

2.1 Bench scale powder reactor system

2.1.1 Gas supply system

The gases used in this thesis are summarized in Table 3. The N_2 carrier gas was supplied from an On-Site Nitrogen generator system (N-30-TGN model) while the other gases, except water vapor, were supplied from gas cylinders acquired from either Praxair or Matheson. The specific flow rates of those gases were controlled by MKS mass flow controllers (MFCs) (model 1179A) which were calibrated with a Bios Definer 220-H digital flow meter. Water vapor was formed by a Bronkhorst water vaporization system that had three components: an El-FLOW MFC for N_2 carrier gas, a LIQUI-FLOW MFC for liquid water, and a controlled evaporator mixer (CEM). Stainless steel tubing was used throughout. The line segments immediately downstream of the MFCs manifold, including all fittings and valves, were heated to around 130-140°C and wrapped in high temperature insulating tape (Darco Southern Tetraglas 3000 Woven Tape) to avoid water condensation.

Table 3 - Gases used in this study

Gas	Description	Purity
N_2	Carrier gas, purge gas for reactor and FTIR	99.999%
O_2	Pure	99.993%
CO	Balanced with N_2	10%
CO_2	Pure	99.999%
NO	Balanced with N_2; corrosive	0.5%
NO_2	Balanced with N_2 and in O_2; corrosive	0.5%
SO_2	Balanced with N_2; corrosive	0.1%
H_2O	Produced from DI water	100%

2.1.2 Reactor system

The reactor system consisted of a 20 in. long quartz tube with 6.35 mm outer diameter and 4 mm inner diameter, and a Lindbergh Mini-mite temperature controlled furnace. Approximately 88 mg of catalyst powder, sandwiched between 2 small quartz wool plugs to maintain bed position, was placed in the quartz tube such that the catalyst bed was within 3 cm from the inlet K-type thermocouple tip and about 3-4 cm from the outlet K-type thermocouple tip. The temperature measurement from the inlet thermocouple was taken as the temperature values in this study. A schematic of reactor tube is shown in Figure 10.

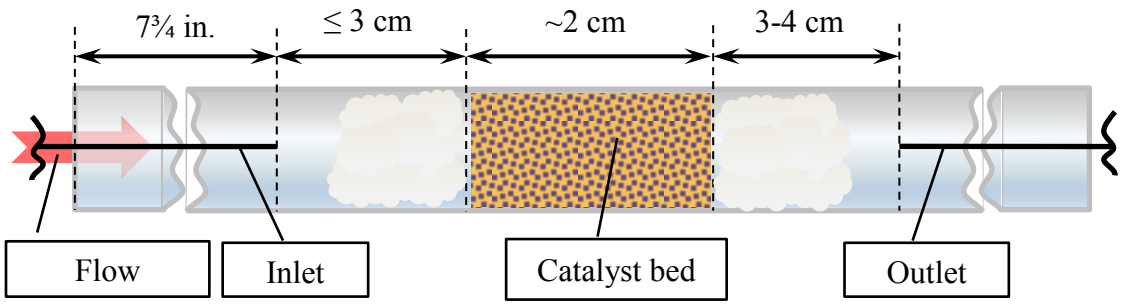

Figure 10 - Schematic view of the reactor tube (not to scale).

The gas supply manifold was divided into two pathways: one going to the reactor tube and the other bypassing the entire furnace set-up. Both pathways meet at a three-way valve, with its outlet leading to a MKS Multigas MG-2030 FTIR spectrometer used to measure gas concentrations (in volumetric ppm). The gas cell inside the spectrometer was maintained at 191°C. The instrument was also in constant purge by a FTIR purge gas produced by Parker Balston. Both gas measurement data and temperature data were monitored real time via Ethernet connection and National Instrument Field point modules, respectively, and collected via MKS MG2000® software and Labview® software, respectively.

2.2 Diffuse Reflectance Infrared Fourier Transform Spectroscopy (DRIFTS)

2.2.1 Background

In-situ DRIFTS is a common surface characterization technique using IR based on vibrational and rotational transition frequencies of diatomic polarized bonds of adsorbed compounds. A sample surface is exposed to an incident IR beam with a range of wavelengths or frequencies. This incident beam penetrates into the sample surface at a certain depth. Beam reflections and absorptions occur in inter-particular space and then rejoin as a single reflectance beam, thus "diffuse reflectance," weaker in intensity due to absorption. Photons at certain frequencies will induce mostly vibrational transitions, and sometimes rotational transitions, of diatomic polarized bonds, and eventually will be absorbed. The reflected IR beam, now with certain frequencies lost or absorbed, is detected by a detector and is measured in voltage, resulting in a plot

called an interferogram. A Fourier transformed interferogram gives a transmittance vs. wavenumber plot, which is then used for surface species identification.

2.2.2 Spectrometer and data acquisition system

The IR source and analyzer consisted of Thermo Scientific Nicolet IS50 FTIR spectrometer equipped with a Mercury Cadmium Telluride (MCT) detector with Cadmium Telluride (CdTe) window and a KBR beam splitter. This detector is reported highly suitable for kinetic study due to its high sensitivity and its ability to maintain the signals regardless of data-acquisition speed. With this setup, the apparatus is capable of identifying all molecular state transitions that occur in the mid-IR region [26]. A water bath at room temperature was placed underneath the reactor as an external cooling system for the reactor cell.

IR spectral information was processed by OMNIC v9.0 software. The Series feature of the software was utilized to capture real-time kinetic spectral data where each recorded spectrum was the average of 5 scans of 4.0-cm^{-1} resolution. The data acquisition rate was as fast as 1.5s/spectrum. All spectra were shown in Kubelka-Munk units, expressed in Eqn. (1 in terms of Reflectance unit (R_∞) or Transmittance unit as

$$KM = \frac{(1 - R_\infty)^2}{2R_\infty}, \qquad \textbf{Eqn. (1)}$$

because it was commonly accepted for diffuse reflectance experiments [27].

In this study, the equation for KM was expressed as followed:

$$KM = \frac{|1 - R_\infty|(1 - R_\infty)}{2R_\infty} \qquad \textbf{Eqn. (2)}$$

to accommodate for the negatively growing IR features which may not be present in background spectra.

2.2.3 Gas supply system and reactor system

The gas supply system resembles the one described in section 2.1.1 of this thesis, except for the carrier gas now being He instead of N_2. The total flow rate was maintained at 50 sccm total. The gases used in DRIFTS experiments were O_2, NO, CO, and He.

Figure 11 shows a schematic of the reactor cell where catalyst sample was prepared as a pellet with 5 mm diameter and 2-3 mm thick. Gas enters the sealed system from a 1/16" nozzle and flows through the catalyst sample before leaving the reactor to vent. This reactor design shows a relatively large dead volume in which stagnant gas is present. This dead volume, initially filled with air, will have to be purged with carrier gas, which was He in this study, before reactant gases are introduced.

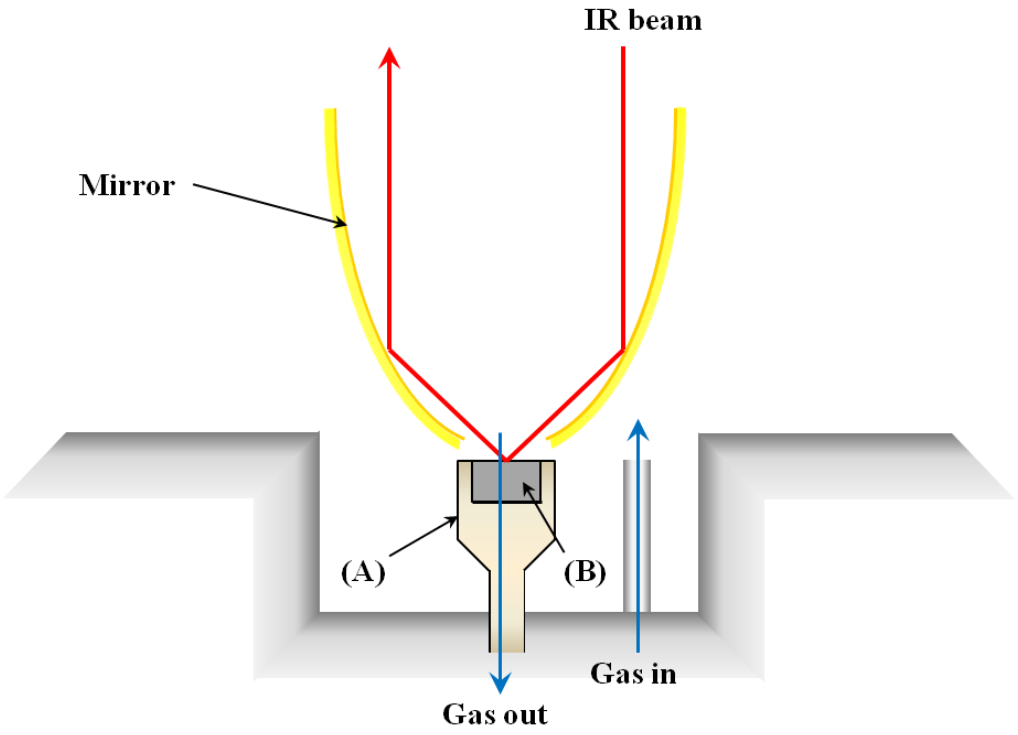

Figure 11 - Schematic view of the reactor. A) Reactor cup. B) Powder sample

2.3 Catalyst preparation - Incipient wetness impregnation and hydrothermal aging

The NH_4-form of β zeolite (Zeolyst, Si:Al ratio = 25) was first dried at 80 °C for 2 h, then at 100 °C for 12 h, and was calcined at 500 °C for 2 h to convert it to H-form. The heating rate was kept at 1°C/min. During calcination, the crucible containing the powder was shaken gently to avoid powder wicking. Immediately after cool-down, the powder was mixed with a $Pd(NO_3)_2$ solution via incipient wetness impregnation, such that the final Pd content was 1wt.% Pd/BEA. Drying and calcination was again performed, following the same temperature profile as above. The sample was hydrothermally treated at 750 °C for 10 h in a 250 sccm total flow of 10% O_2 and 10% H_2O with a N_2 balance. The heating rate (to 750°C) was kept at 5°C/min to avoid overshooting.

Chapter 3 – Effect of CO on Pd/BEA Passive NOx Adsorbers

The content of this chapter is directly from a published paper [28]. However, in-text citations were adjusted for bibliography coherency.

3.1 Introduction

NO_x emission reduction in diesel engine exhaust is challenging [29]. Selective catalytic reduction (SCR) and NO_x storage and reduction (NSR) have been extensively studied as potential solutions and both technologies have been commercially proven and have high NO_x reduction efficiencies [1,6,30,31]. However, their performance is constrained at low temperatures, and because of these limitations, most NO_x will slip through the aftertreatment system when the catalyst temperatures are below approximately 200 °C. Such low temperatures are associated with cold-start emissions and can constitute a major portion of the total NO_x emitted during a drive cycle. One strategy to mitigate cold-start emissions is to store NO_x at low temperature then release it for downstream reduction when the exhaust temperature surpasses 200 °C. Passive NO_x adsorbers have been designed and developed to do just this [16].

NO_x adsorption has been well studied in the context of lean NO_x traps (LNTs) [1,32–35]. However, the LNT design includes the stored NO_x being reduced to N_2 when exposed to a fuel (or reductant) rich gas. For passive NO_x adsorber systems, the gas phase is assumed to be always fuel lean and NO_x is to be reduced on downstream catalytic components. Studies have shown promising passive NO_x adsorbers ranging from mixtures of transition metal oxides to metal-containing zeolites [17–20]. Others have incorporated precious metals on alumina to store and release NO_x under oxidizing conditions [21,22]. Ji et al. studied Pt/Al_2O_3as well as $Pt/La/Al_2O_3$ as potential passive

NO_x adsorbers [22]. They found that the addition of La to Pt/Al_2O_3 improved NO_x storage at low temperature by enhancing nitrate formation. However, this limited NO_x desorption below 250 °C, in other words the nitrates may be too stable to be released in a more ideal temperature range. NO_x storage on ceria-based catalysts doped with Pd, Pt, and rare earth elements was studied, and Pd/CeO_2 loaded with 20 mol% Pr had significant NO_x storage at 120 °C and NO_x release below 350 °C [25]. In terms of zeolite based adsorbers, Chen et al. compared Pd catalysts supported on CeO_2 and MFI, CHA, and BEA zeolites [20]. All four catalysts showed considerable NO_x storage and desorption efficiencies. However, Pd/BEA appeared better than the other catalysts in terms of NO_x storage at 100 °C or lower and NO_x release above 200 °C.

Though there has been extensive research targeting improved cold-start catalysts, emissions at low temperature are still an issue. The passive NO_x adsorber (PNA) technology appears to be a relevant strategy to mitigate low temperature NO_x emissions. In this study, we chose Pd/BEA as a model passive NO_x adsorber material and evaluated the impact of CO on NO_x adsorption and desorption. Diffuse reflectance infrared Fourier transform spectroscopy (DRIFTS) was used to characterize Pd states in an attempt to understand the reaction chemistry.

3.2 Experimental Methods

3.2.1 Catalyst preparation

The NH_4-form of β zeolite (Zeolyst, Si:Al ratio = 25) was first dried at 80 °C for 2 h, then at 100 °C for 12 h, and was calcined at 500 °C for 2 h to convert it to H-form. Immediately after cool-down, the powder was mixed with a $Pd(NO_3)_2$ solution via incipient wetness impregnation, such that the final Pd content was 1wt.% Pd/BEA.

Drying and calcination was again performed, following the same temperature profile as above. The sample was hydrothermally treated at 750 °C for 10 h in a 250 sccm total flow of 10% O_2 and 10% H_2O with a N_2 balance.

3.2.2 Reaction conditions

Approximately 88 mg of this Pd/BEA powder were placed in a micro-reactor which was placed inside a Thermo Fischer Lindberg Minimite furnace. In all experiments, the catalyst was preconditioned at 500 °C in 10% O_2 before it was cooled down to the adsorption temperature, which was 80 °C in this study. The temperature was measured ~1 cm upstream of the catalyst bed using a K-type thermocouple. Pretreated Pd/BEA was then exposed to various feed streams composed of 186 ppm NO, 5% H_2O, 10% O_2, with a balance of N_2. The inclusion of CO, NO_2 and CO_2 was also investigated. The adsorption phase was 100 s at 80 °C and was followed by a ~63 °C/min heating ramp to 500 °C. The effluent stream was monitored by an MKS Multigas 2030 FTIR. In this study, all NO_x concentration measurements presented are the summation of NO and NO_2 concentrations.

3.2.3 Diffuse Reflectance Infrared Fourier Transform Spectroscopy (DRIFTS)

Approximately 50 mg of Pd/BEA sample was pressed into a pellet before it was loaded into a Smart Collector DRIFTS cell, set in a Nicolet IS50 IR spectrometer with a MCT-highD detector. Spectra were collected at a resolution of 4 cm^{-1}. Catalyst samples were pretreated in 10% O_2/He at 500 °C for 1 h before they were cooled down to 80 °C in O_2 for subsequent experiments. Adsorption experiments were carried out using a total flow of 50 sccm containing 200 ppm NO and/or 800 ppm CO in a balance of He.

3.3 Diffuse Reflectance Infrared Fourier Transform Spectroscopy (DRIFTS)

3.3.1 Effect of gas components

We here define the base case as that containing NO, O_2, H_2O in a balance of N_2. The experiment consisted of an adsorption phase that began at t = 60 s in Figure 12. The adsorption phase lasted 100 s. The concentration data obtained from the base case is shown in Figure 12A, as are the results demonstrating the effect of CO concentration on NO_x uptake activity. The amounts of adsorbed NO_x are listed in Table 4. At t = 60 s, the Pd/BEA material adsorbed the entering NO until the available sites were saturated, generating a relatively standard adsorption profile. The HBEA zeolite was also evaluated and as shown, adsorbed little NO. Compared to the base feed case, the addition of CO generally enhanced NO_x uptake over the Pd-containing samples, though the beneficial effect was not noticeable until more than 100 ppm CO was added. During this adsorption phase, a transient in CO_2 concentration was detected (Figure 12B) and the amount formed increased with increasing inlet CO concentration. CO_2 was not observed when evaluating the HBEA.

Note, the CO_2 evolved, and thus the CO oxidation, was transient, and was correlated to NO_x uptake. Also, with CO in the feedstream the amount of NO that adsorbed was consistently more than the amount that desorbed, with an increasing difference with increasing CO amount. These results demonstrate that NO reduction occurred, even at 80 °C, via a Pd-catalyzed reaction. Note, no N_2O was observed.

Although adsorption quantities are important, the range of temperatures where desorption occurs is just as critical. NO_x should desorb at temperatures above the

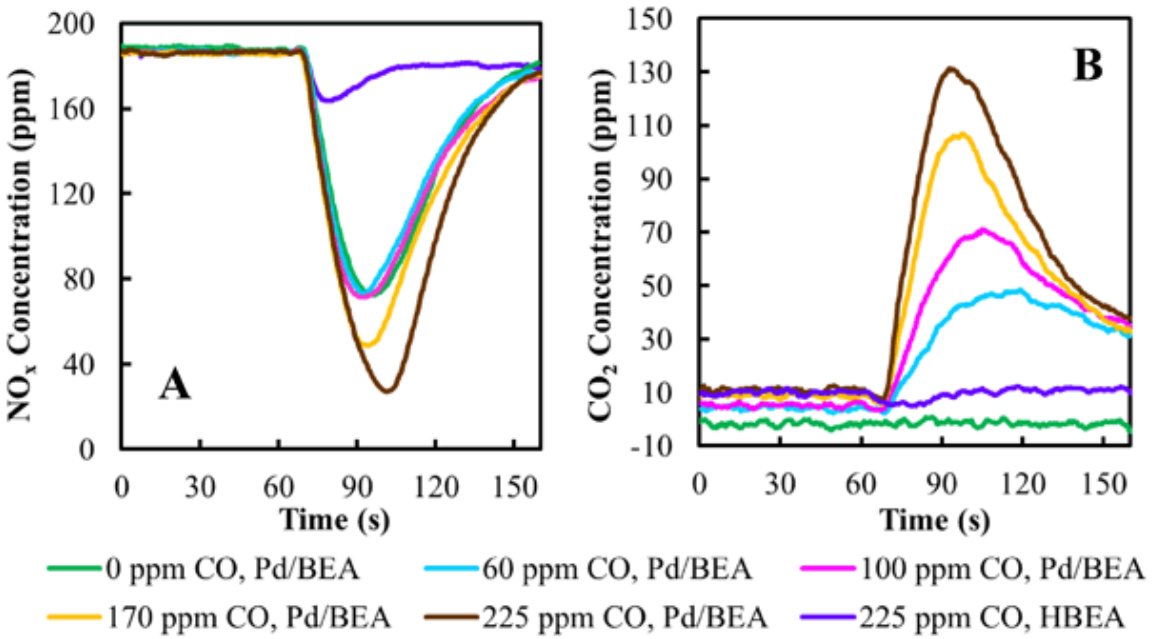

Figure 12 - A Effect of CO on NO_x uptake and **B** CO_2 detected. The feedstream was switched to the reactor at t = 60 s. The inlet stream consisted of 186 ppm NO, 10% O_2, 5% H_2O, various CO amounts and a balance of N_2

Table 4 - NO_x adsorption and desorption ($\mu mol_{NOx}/g_{cat}$) as a function of CO concentration and the presence of NO_2 and CO_2. Numbers in parentheses are the NO_x:Pd ratios

186 ppm NO, 10% O_2, 5% H_2O, and	**NO_x Adsorbed**	**NO_x Desorbed**
0 ppm CO	14 (1.7)	14 (1.7)
60 ppm CO	13 (1.6)	10 (1.2)
100 ppm CO	15 (1.8)	11 (1.3)
170 ppm CO	17 (2.0)	13 (1.5)
225 ppm CO	20 (2.4)	15 (1.8)
93 ppm NO, 93 ppm NO_2, 5% H_2O	17 (2.0)	13 (1.6)
2.5% CO_2, 5% H_2O	14 (1.7)	13 (1.6)

temperature required for NO_x reduction over downstream NO_x reduction catalysts. However, the onset of NO_x desorption should not be at too high of a temperature,

otherwise regeneration or removal of NO_x from the PNA for later adsorption would be challenging. And depending on the engine, this might require strategies to achieve higher temperatures than normal and thus incur a fuel penalty. The NO_x concentrations measured during the temperature programmed desorption (TPD) phase after the adsorption at 80 °C, in the absence of CO and with different CO amounts added, are shown in Figure 13. In the absence of CO, the NO_x desorption peak locations, at approximately 100 °C (peak A) and 180 °C (peak B), should be considered too low. Downstream NO_x reduction catalysts operate efficiently at temperatures above ~180–200 °C. However, when CO was included in the feed, a new high temperature release feature appeared, and the majority of NO_x desorption occurred in this higher temperature region. Peaks include a shoulder at around 160 °C (peak B), a peak at 260 °C (peak C), and small broad peak at 430 °C (peak D). As the CO concentration increased, peaks C and D grew, whereas peak B shrank. Therefore, CO led to increased adsorbed NO_x thermal stability. As will be shown below, this is due to CO's ability to reduce Pd to a lower oxidation state, which leads to the more strongly adsorbed species. The influence of NO_2 and CO_2 were also evaluated with summary data listed in Table 4 and the TPD results shown in Figure 14. CO_2 did not have an impact. With NO_2 added, a larger amount of the low temperature species, peak A, was measured, while peak B decreased in intensity. The influence of NO_2, like CO, is related to its influence on the Pd oxidation state, here keeping it in a higher oxidation state as NO_2 is a known strong oxidant.

3.3.2 NO adsorption characterized by DRIFTS

As shown above, CO changed the surface chemistry of Pd/BEA such that more NO_x

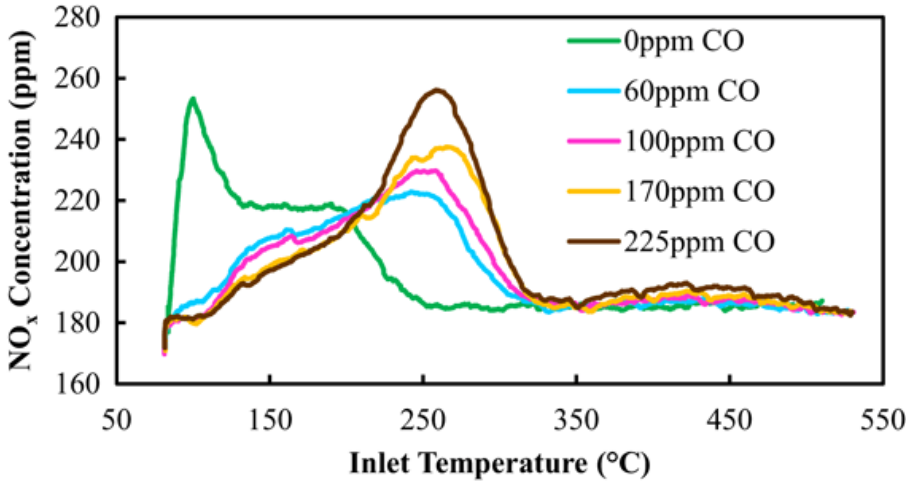

Figure 13 - Effect of CO concentration on NO_x-TPD after the adsorption described in Figure 12. The inlet stream consisted of 186 ppm NO, 10% O_2, 5% H_2O, various CO amounts and a balance of N_2. The ramp rate was 60 °C/min

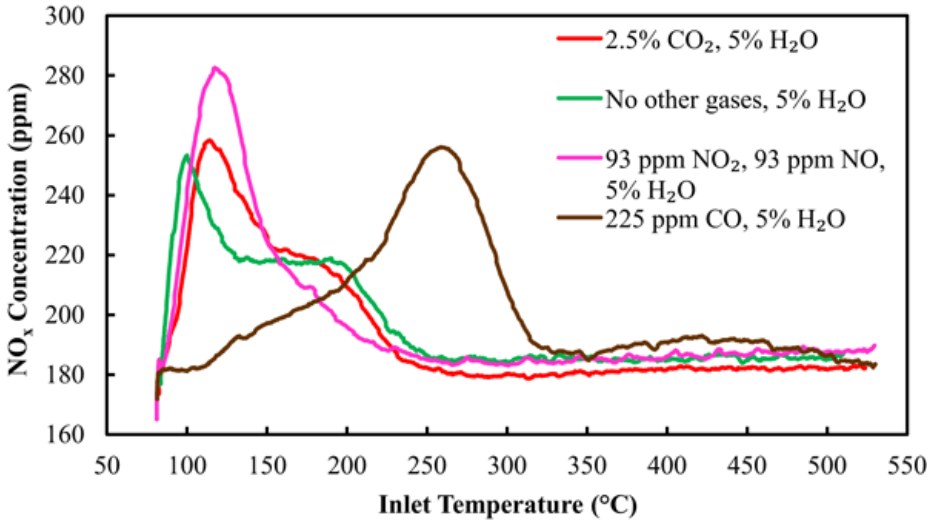

Figure 14 - Effect of NO_2 and CO_2 on NO_x desorption. The feedstream was switched to the reactor at t = 60 s. The inlet stream consisted of 186 ppm NO or 93 ppm NO and 93 ppm NO_2, 10% O_2, 5% H_2O, 0 or 5% CO_2 and a balance of N_2

adsorbed and the desorption characteristics changed. In an attempt to understand why, DRIFTS was used to characterize the interactions between Pd/BEA and NO and CO. First, CO adsorption on an O_2-pretreated Pd/BEA sample at 80 °C was characterized in order to help identify what Pd states exist, and multiple IR features (Figure S1) were observed. The assignments, based on literature values, for each CO peak can be found

in Table 5. These data demonstrate that there were not only multiple Pd states, but also multiple types of binding sites for those similar chemical states.

Table 5 - Peak assignments used in this study [36,37]

IR features (cm^{-1})	**Assignment**
1779	$(NO)_2$ dimer symmetric stretch on Pd
1826	NO symmetric stretch of dinitrosyl species (NO–Pd–NO)
1855	$(NO)_2$ dimer asymmetric stretch on Pd
2077	Linear CO on low coordination Pd^0
2098	Linear CO on terraces of Pd^0
2118	Linear CO on Pd^+
2137	Linear CO on ionic Pd
2152	Linear CO on Pd^{2+}
2179	Linear CO on highly dispersed Pd^{2+}

In terms of NO_x uptake, the sample was exposed to NO + O_2, and IR spectra were collected until no changes were observed, after which CO was introduced. Figure 15 shows NO adsorption spectra with NO and O_2 exposure at 80 °C. Peaks at 1806, 1815, 1826, 1847, 1874, and 1889 cm^{-1} were observed. The bands at 1826 and 1874 cm^{-1} can be assigned to the N = O symmetric stretch of palladium-dinitrosyl species and asymmetric stretch of an $(NO)_2$ dimer on Pd, respectively [36]. The rest of the IR features are assigned to N–O bond vibrations in a palladium-nitrosyl complex. This N–O bond is sensitive to the chemical state of Pd. Since Pd initially existed in multiple oxidation states, the multiple bands associated with NO exposure show that NO could bind to multiple Pd sites/states. Available, literature-based peak assignments are listed in Table 5.

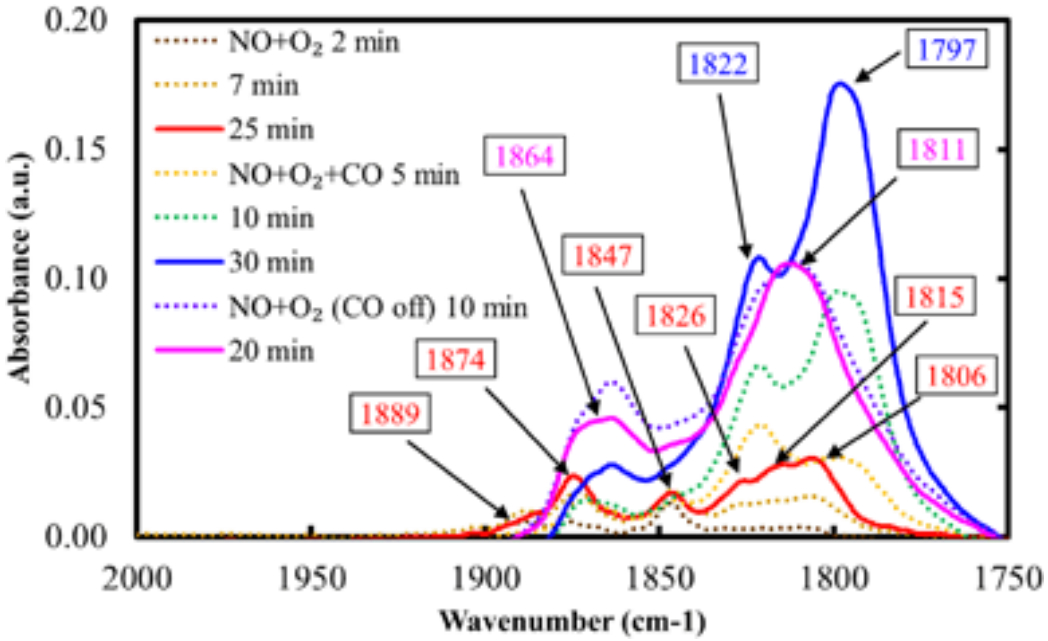

Figure 15 - DRIFTS spectra obtained during Pd/BEA exposure to NO + O_2, then NO + CO + O_2, then NO + O_2 (i.e. CO was turned off)

After the IR signals no longer changed, i.e. NO adsorption saturation was achieved, CO was introduced and the peaks at 1822 and 1797 cm^{-1} increased substantially/appeared whereas the peaks at 1847, 1874, and 1889 cm^{-1} decreased slightly. The peak at 1822 cm^{-1} represents dinitrosyl species whereas 1797 cm^{-1} is close to the $(NO)_2$ symmetric stretch, which has been reported at 1779 cm^{-1}. The shift in peak location is likely due to the ionic or oxidized states of Pd in this study whereas the reported wavenumbers are associated with a Pd(111) surface [36]. This new feature indicates a new site for adsorption, which should therefore lead to a different binding energy—all of which coincides well with the data observed with the addition of CO in the reactor experiments. CO led to more NO_x adsorbed, and to desorption at higher temperatures. These new, lower wavenumber features, likely associated with reduced Pd, are responsible for the increased capacity and more stable NO bound species. Lastly, as shown in Figure 15, when CO was turned off, the 1797 cm^{-1} feature

disappeared and the 1822 cm^{-1} feature decreased in intensity. The IR band at 1811 cm^{-1}, however, remained and was substantially larger than any features prior to CO addition. This suggests that CO stabilized the NO bound to the Pd. At the same time, in the zeolitic T–O–T vibration wavenumber region, a negative peak was detected around 933 cm^{-1} (Figure 16), which was not observed with exposure to just NO. This negative feature indicates less T–O–T perturbation by the exchanged Pd ions [20], possibly due to their reduction to lower oxidation states. NO + O_2 exposure did not induce changes in this region, demonstrating that it did not alter Pd oxidation states compared to the background. CO as a reductant could lower the Pd oxidation state and induce this change. However, it was not clear if the reduction was complete to metallic Pd, or partial reduction to lower (but non-zero) oxidation states. In order to clarify this, H_2 was used as a preconditioning gas instead of O_2. Such a reductive pretreatment should further reduce Pd to even lower oxidation states than reduction by CO in the presence of O_2. Figure S2 shows NO adsorption on H_2-reduced Pd/BEA at 80 °C. Only one peak at 1749 cm^{-1} was observed, most likely representing the nitrosyl vibration on metallic Pd [38]. This IR feature was not present during any experiments with the oxidatively pretreated sample. Therefore, it was unlikely CO reduced Pd to its metallic form.

The above experimental data show beneficial effects of CO on NO_x uptake at low temperature and preferential release of NO_x after 200 °C, where downstream NO_x reduction catalysts achieve appreciable performance. CO apparently enhanced NO_x adsorption and binding strength by reducing Pd to lower oxidation states. Once reduced, Pd gains electrons in its valence orbitals. We speculate that because the metal-nitrosyl bond involves π-back-donation of these valent electrons to partially filled

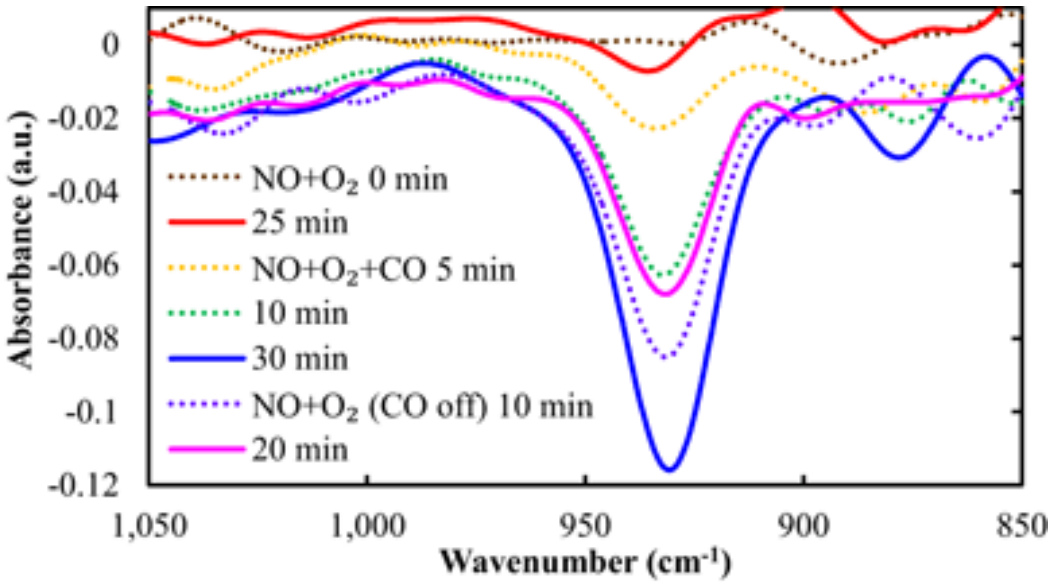

Figure 16 - DRIFTS spectra obtained during Pd/BEA exposure to NO + O_2, then NO + CO + O_2, then NO + O_2 (i.e., CO was turned off). Low wavenumber region

orbitals of NO molecules, this electron gain further facilitates back-donation, thereby strengthening the Pd–N bonds.

DRIFTS experiments revealed the importance of the oxidation state of Pd in NO_x storage and release activity. As shown above, when NO_2 or CO was included in the feed, changes in peak amplitude and position were evident. Compared to the TPD pattern under the basic feed case, peak A was larger in the presence of NO_2, a stronger oxidant than O_2, whereas peak B was smaller. In the case with CO_2, neutral in regards to the chemical state of Pd, no change in peak amplitude was observed. It is therefore very likely that peak A, the NO desorbing from the less stable site, is associated with Pd species in a high oxidation state and peak B the next lower oxidation state. This assignment is further supported by the disappearance of peak A and the decrease of peak B in the presence of reductant CO. The addition of CO also led to the formation of peaks C and D, the higher temperature NO_x desorbing peaks. These could therefore be associated with NO_x species on Pd at even lower oxidation states. Also of note, the

NO_x to Pd ratio (Table 4) was always larger than 1, which either suggests adsorption on the zeolite or that Pd adsorbed more than one NO molecule. The DRIFTS results show that there was dinitrosyl and $(NO)_2$ dimer on Pd formation, and the HBEA sample trapped little if any NO, supporting the >1 NO:Pd ratio being explained by dintrosyl or dimer formation.

3.4 Conclusions

In this study, the effect of CO on NO_x storage and release on/from Pd/BEA was characterized. CO resulted in increased NO_x uptake at low temperature, as well as inducing desorption at higher temperatures. DRIFTS results indicate that the chemical state of the Pd is the key factor. Pd at lower oxidation states can bond NO_x more strongly via the strengthening of the covalent bond by π-backdonation from Pd as the metal gains more electrons.

Chapter 4 – Effect of SO_2 on Pd/BEA Passive NO_x Adsorbers

4.1 Introduction

Though the influence of sulfur/sulfation has been investigated in the context of SCR and LNT catalysts, that on passive NO_x adsorbers in general has not been well-established [39,40]. The stereotypical consensus regarding SO_2 effects is that it will negatively impact a catalyst's performance to various extents from mild to complete deactivation. In terms of passive NO_x adsorbers, Chen et al. has shown decreased NO_x uptake capacity on sulfated Pd-based catalysts supported on CeO_2 and MFI, CHA, and BEA zeolites, among which Pd/CeO_2 barely shows any NO_x uptake after sulfation, as shown in Figure 17. Contrary to Pd/CeO_2, Pd/zeolite catalysts were not severely affected by sulfation. Though according to the authors sulfur is known to interact strongly with PdO_2, the prevalence of highly dispersed Pd over Pd oxides accounts for the strong sulfur tolerance of Pd/zeolites, and the mild reduction in NO_x storage capacity is probably attributed to the small amount of PdO. It is noted that the catalysts were initially treated with 100 ppm SO_2, 10% O_2, 5% H_2O, and 5% CO at 300°C until 21 mol of SO_2 per mole of Pd was achieved [20].

However, the NO_x desorption activity on sulfated samples was not discussed in detail in the above study. Therefore, this thesis will provide a more complete picture into the effect of SO_2 on Pd/BEA passive NO_x adsorbers.

4.2 Experimental Methods

Temperature programmed desorption (TPD) experiments were performed in a bench-top flow reactor on hydrothermally aged 1% Pd/BEA. The catalyst was

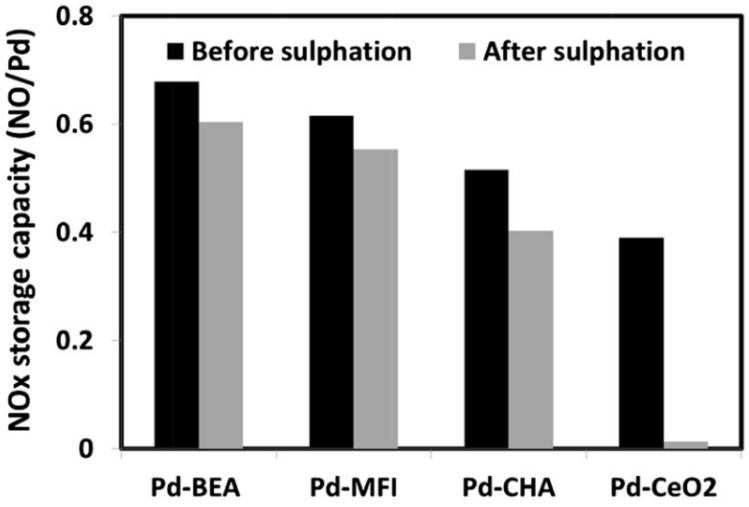

Figure 17 - Effect of sulphation on the NO storage capacity at 100°C for different 1 wt.% Pd samples [20]

pretreated in 10% O_2 at 500°C before it was cooled down to 80°C for adsorption. Preconditioned Pd/BEA was exposed to the same feed stream as used in chapter 3 with 0 or 225 ppm CO, and with the addition of 50 ppm SO_2 in both adsorption and desorption phases. The TPD procedure remains the same with 100s adsorption and a heating rate of ~66°C/min to 500°C.

4.3 Results and Discussions

Similar to the experimental protocol in chapter 3, the adsorption started at t = 60 s in Figure 12. This set of TPD experiments shows little to no SO_2 effect on both NO_x uptake and release. In the presence of CO, the amount adsorbed was reduced by 19%, and the amount desorbed was reduced by 22%. Both desorption peaks at ~250°C and 450°C show decreased amplitude in SO_2 compared to those without SO_2. This small SO_2 effect agrees with what Chen et al. found. Moreover, the peak locations and shapes remain unchanged under the influence of SO_2.

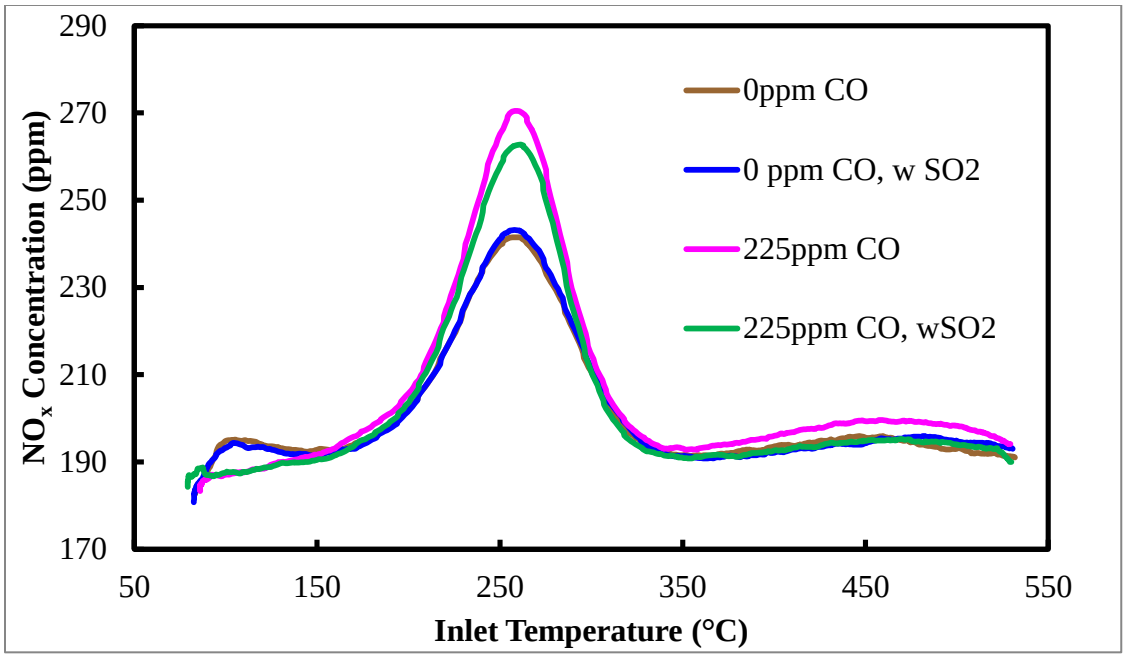

Figure 18 - Effect of SO_2 on NO_x desorption activity

Table 6 - Adsorption and desorption amount of NO_x under feed gases with vs. without SO_2

$\mu mol_{NO_x}/g_{cat}$	**No CO**	**With SO_2 No CO**	**225ppm CO**	**225ppm CO, with SO_2**
Adsorption	13.9	13.9	15.3	18.5
Desorption	13.0	11.9	13.8	17.7

4.4 Conclusions

The influence of SO_2 was shown in this study by temperature programmed desorption experiments. Though it hinders NO_x activity to a small extent, SO_2 overall does not alter the uptake or release of NO_x on Pd/BEA passive NO_x adsorber.

Chapter 5 – Desorption Kinetics of NO_x on Pd/BEA – Effect of Heating Rate

5.1 Introduction

One of the key features in passive NO_x adsorbers is the desorption temperature. An effective passive NO_x adsorber should start the NO_x release no earlier than approximately 200°C. Thermal desorption is influenced by many factors, which can be associated with the catalyst, the gas feed, or the experimental conditions. Interestingly, it has been well established that the temperature at which desorption occurs can be altered systematically by varying the heating rate, a feature related to the experimental protocol. In fact, the heating rate can be related to the peak temperature location in a temperature programmed desorption (TPD) experiment by the following expression derived from the Polanyi-Wigner equation:

$$\beta = g'(\theta)|_{T_p} \nu_n \frac{RT_p^2}{E_d} exp\left(-\frac{E_d}{RT_p}\right), \qquad \textbf{Eqn. (3)}$$

in which β is the heating rate; $g'(\theta)$, the first derivative of surface coverage at peak temperature T_p; ν_n, pre-exponential factor; R, universal gas constant; T_p, desorption peak temperature; E_d, desorption activation energy; and n, desorption order.

The objective of this study is to investigate how heating rate affects the NO_x thermal desorption activity. The Polanyi-Wigner equation will be used as a model in this study.

5.2 Experimental Methods

Temperature programmed desorption (TPD) experiments were performed in a bench-top flow reactor on hydrothermally aged 1% Pd/BEA. The catalyst was pretreated in 10% O_2 at 500°C before it was cooled down to 80°C for adsorption.

Preconditioned Pd/BEA was exposed to the same feed stream as used in chapter 3 with 225 ppm CO. The TPD procedure remains the same with 100 s adsorption but with various heating rates to 500°C.

5.3 Results and Discussions

5.3.1 Desorption kinetics from heating rate method – Polanyi-Wigner model

The effect of heating rate is shown in Figure 19. The peak area appears smaller as the heating rate decreases and may suggest lower desorption amounts. However, it must be noted that slower heating rate requires more time to reach the target temperature. Thus, time-accumulative amounts of NO_x desorbed are the same regardless of heating rate. As the heating rate decreases, the peak temperature location also shifts to lower values. This is however expected by the Polanyi-Wigner model, according to which the heating rate β and the peak temperature location T_p are positively correlated. This correlation can give rise to the evaluation of a desorption energy, E_d. Eqn. (3 can be rearranged to:

$$ln\left(\frac{\beta}{T_p^2}\right) = ln\left[g'(\theta)\frac{Rv_n}{E_d}\right] - \frac{E_d}{R}\cdot\frac{1}{T_p}. \qquad \textbf{Eqn. (4)}$$

A plot of $\ln\left(\frac{\beta}{T_p^2}\right)$ vs. $\frac{1}{T_p}$ yields $-\frac{E_d}{R}$ as the slope.

For a more accurate analysis, the largest peak, which lies between 200 – 300°C, was selected. With T_p obtained from the peak deconvolution, as shown in Figure 20, and the heating rate β from temperature profiles, $\ln\left(\frac{\beta}{T_p^2}\right)$ vs. $\frac{1}{T_p}$ is plotted (Figure 21) to obtain a

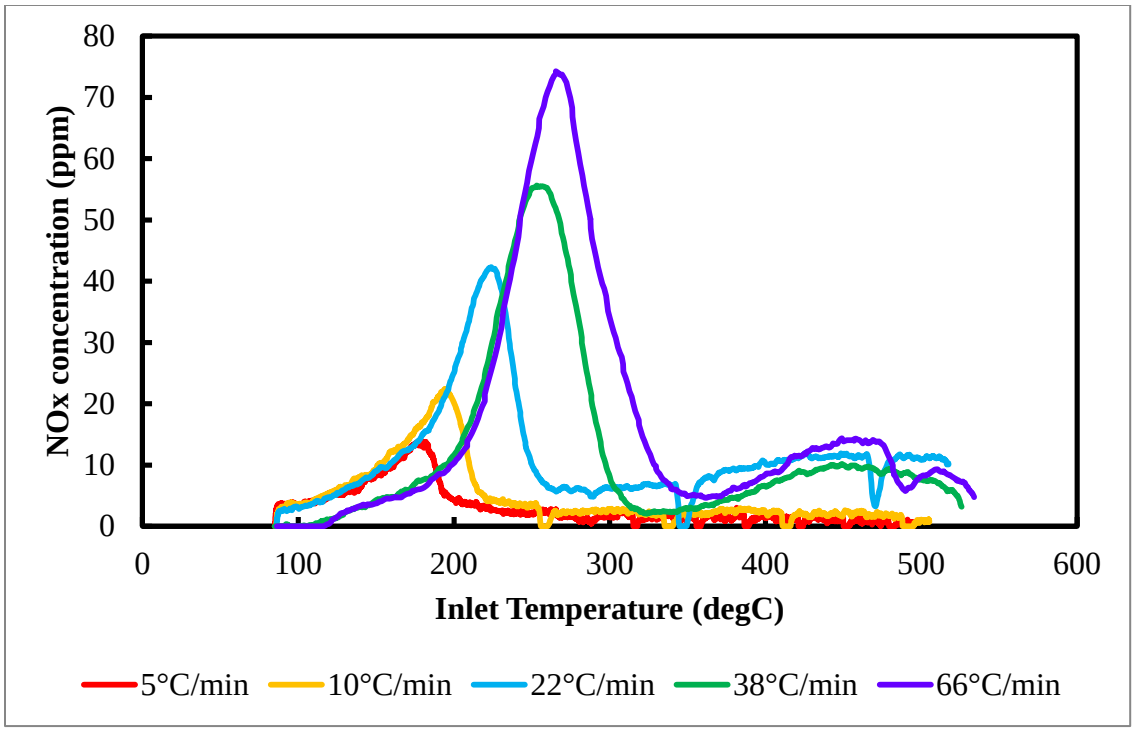

Figure 19 - NO_x-TPD profiles under various heating rate

desorption barrier of 46.0 kJ/mol from the slope. This desorption activation energy, which is assumed independent of surface coverage, is only apparent and representative of the surface species that causes the desorption peak of interest.

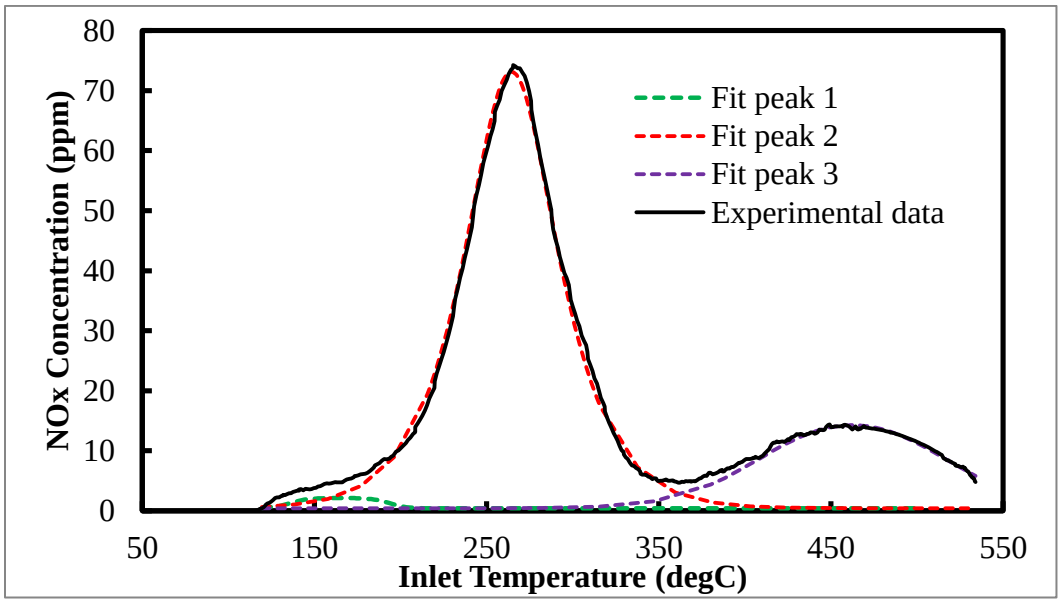

Figure 20 - Peak deconvolution of the TPD spectrum with $\boldsymbol{\beta}$ = 66°C/min

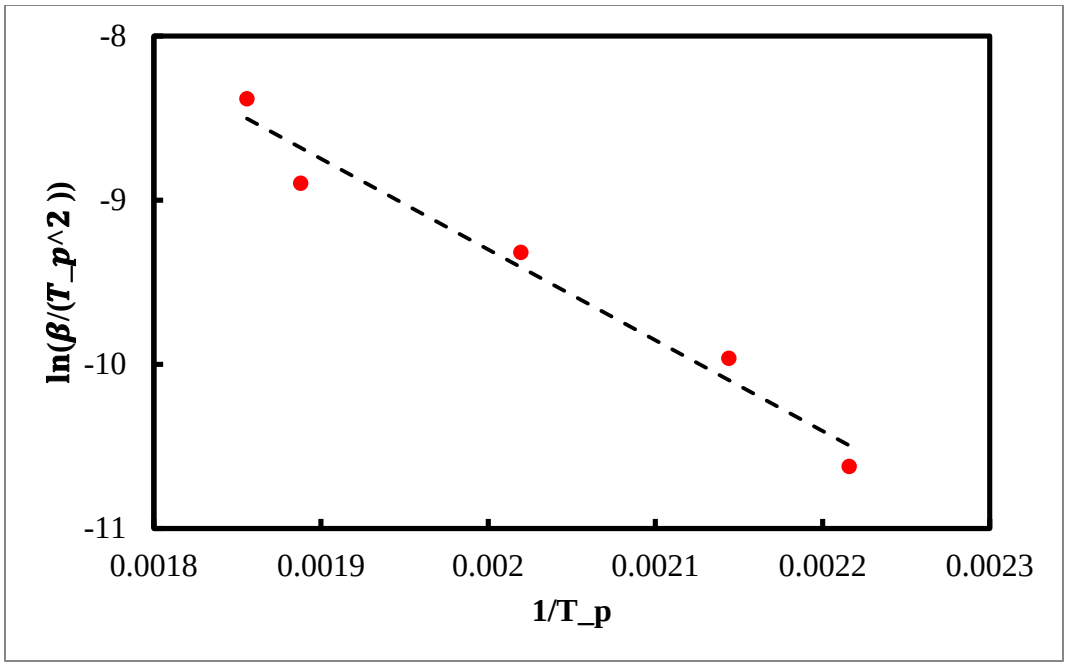

Figure 21 - ln $\left(\frac{\beta}{T_p^2}\right)$ vs. $\frac{1}{T_p}$ plot

The remaining kinetic terms yet to resolve in Eqn. (3 are the pre-exponential factor ν_n, $g'(\theta)$, and desorption order n. The first two terms can be functions of surface coverage. However, Eqn. (3 is specific to the moment when the desorption rate reaches a maximum. As a result, surface coverage will be at a certain value, which will render both ν_n and $g'(\theta)$ constant. The pre-exponential factor ν_n can be calculated directly from Redhead's method using the following expression:

$$\nu_n = \frac{E_d \beta}{R T_p^2 \theta_0^{n-1}} exp\left(\frac{E_d}{R T_p}\right), \qquad \textbf{Eqn. (5)}$$

where θ_0 represents the initial coverage. This equation however assumes ν_n independent of surface coverage and requires θ_0 and n to calculate ν_n. The initial coverage θ_0 can be calculated from the adsorption amount in the TPD spectra. However, since the available active sites are associated with Pd only and not on zeolite support, as shown via DRIFTS results in chapter 3, θ_0 is computed as followed:

$$\theta_0 = \frac{Total\ NOx\ adsorbed\ (mol)}{Total\ amount\ of\ Pd\ (mol)} \qquad \textbf{Eqn. (6)}$$

A ratio of NO_x:Pd of 1:1 was assumed in Eqn. (6. The initial coverage was slightly different for each experiment. Therefore, the pre-exponential factor will be calculated for each TPD spectrum using the respective θ_0 instead of the averaged θ_0 and will be reported as the average value. Finally, the desorption is second-order due to the approximately symmetrical peak [41]. All parameters are reported in Table 7.

Table 7 - Desorption kinetic parameters

Parameters	**Heating rate method**
E_d [kJ/mol]	45.95
θ_0	0.16 ± 0.01
n	2
$g'(\theta) \cdot \nu_n$ [s^{-1}]	32230 ± 2227
ν_n [s^{-1}]	3529 ± 353

Among all calculated parameters, the pre-exponential factor does not appear reasonable because it usually ranges from $10^8 – 10^{13}$ s^{-1}. Since the heating rate and the peak temperature location are given directly from experimental data and cannot be changed, the remaining parameters that could be altered to make ν_n more practical are E_d and θ_0. Though computed directly from experimental data, the initial coverage still bears the assumption of NO_x:Pd equal 1:1. This ratio could be 2:1 in the case of $(NO)_2$ dimers bound to Pd, but this would not change ν_n significantly. In order for ν_n to be in the reasonable range, θ_0 has to be between $10^{-6} – 10^{-11}$, which contradicts the remarkable NO_x storage capacity of Pd/BEA. Therefore, the desorption activation energy becomes problematic, even though it seems reasonable.

5.3.2 Peak width analysis – Verification of E_d and ν_n

To verify E_d, a peak width analysis method, developed by Chan et al., was employed [41]. According to this method, E_d can be computed given T_p, the desorption order n, and either the half-width $W_{1/2}$ or the three-quarter width $W_{3/4}$ of a desorption peak. For second-order desorption, E_d is given by following empirical formulas:

$$E_d = 2RT_p\left[-1+\sqrt{1+3.117\left(\frac{T_p}{W_{1/2}}\right)^2}\right] \\ = 2RT_p\left[-1+\sqrt{1+1.209\left(\frac{T_p}{W_{3/4}}\right)^2}\right]. \quad \textbf{Eqn. (7)}$$

The pre-exponential factor ν_n can be subsequently calculated by Eqn. (8, as followed [42]:

$$\nu_n = \frac{\beta E_d^2}{\theta_{0,i} R^2 T_p^3\left(\frac{E_d}{RT_P}+2\right)} \cdot \exp\left(\frac{E_d}{RT_p}\right). \quad \textbf{Eqn. (8)}$$

The half-width and three-quarter-width of the peak of interest can be obtained from the peak deconvolution. It is noted that $\theta_{0,i}$ the initial coverage *for the respective desorption species* (since there are 3 peaks). The newly computed E_d and ν_n are more reasonable compared to the values provided by the heating rate method. The peak width analysis results in a set of E_d and ν_n for one desorption curve. It is noted however that each TPD spectrum resulted in a different set of E_d and ν_n, indicating their non-independency of coverage, which is understandable under this complex system. Table 8 summarized the new values for E_d and ν_n.

Table 8 - E_d and ν_n computed from peak width analysis

Heating rate	**5°C/min**	**10°C/min**	**22°C/min**	**38°C/min**	**66°C/min**
E_d [kJ/mol]	278.2	258.7	186.1	143.7	126.1
ν_n [s^{-1}]	1.5×10^{31}	1.3×10^{28}	9.2×10^{18}	3.0×10^{13}	5.3×10^{11}

The changing in activation energy of desorption and frequency factor with varying heating rate is not explainable by Polanyi-Wigner model, which assumes E_d and ν_n coverage independent. However, for complex system like this, it is worth taking into account the two well-known and discussed effects of compensation and lateral interactions among adsorbates. They are respectively formulated as

$$\ln \nu_n(\theta) = bE_d(\theta) + c = \frac{\Delta E_d(\theta)}{RT_c} + c \text{ and} \qquad \textbf{Eqn. (9)}$$

$$E_d(\theta) = E_{d,0} + \Delta E_d(\theta) = E_{d,0} - W \cdot \theta. \qquad \textbf{Eqn. (10)}$$

For pairwise interactions, we will have the second equation of Eqn. (10, where W represents the interaction energy. W is negative if the interaction is attractive, and is positive if the interaction is repulsive [43].

Interestingly, a plot of $\ln \nu_n(\theta)$ vs. $E_d(\theta)$ using the values in Table 8 resulted in a straight line in Figure 22. The same linear relationship was also established for peaks 1 and 3. Since peak 3 were not clearly visible in experiments with β = 5 and 10°C/min, only data from the remaining 3 experiments were used for peak 1 and peak 3 analysis. Consequently, this relationship allows for the prediction of the frequency factors and activation energies of desorption for experiments with heating rates that fall within the limits of this study. Extrapolation though not recommended but could be used to obtain reference values for heating rates outside the scope of this study.

Though the data points appear to correlate very well, it needs to be mentioned that some pre-exponential factors of the thermal desorption with heating rates close to the limits become too large to be practical, e.g. the ν_n for peak 2 of experiments with β = 5 and 10°C/min in Table 8. This reveals the known disadvantage of the peak width analysis, that it cannot fully unravel the intrinsic ν_n and E_d of a system where those values are coverage dependent. As a result, true understanding of Pd/BEA for its PNA application still remains unknown.

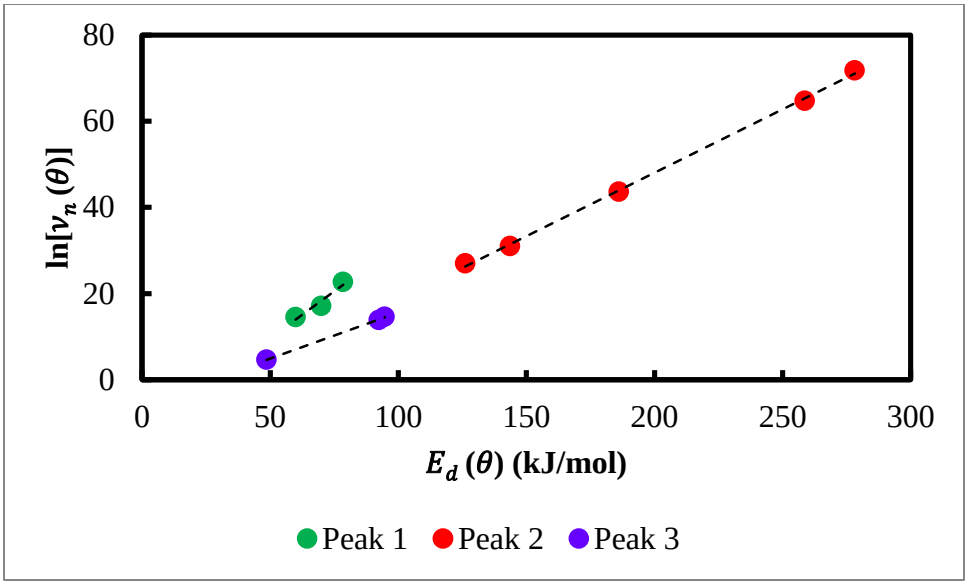

Figure 22 - Compensation effect plot of $\ln \nu_n(\theta)$ vs. $E_d(\theta)$

5.3.3 Simulation of temperature-programmed desorption spectra – Polanyi-Wigner/Peak width analysis model

The discrepancy in desorption barriers and pre-exponential factors in this analysis has led to another necessary step of verification. Thus, we attempt to reconstruct the TPD spectra using the desorption kinetic parameters obtained in the previous sections using Polanyi-Wigner model. The expression for desorption rate for the respective desorption species is:

$$r_i = -\frac{d\theta}{dt} = \nu_2 \theta_i^2 \exp\left(-\frac{E_d}{RT}\right). \qquad \textbf{Eqn. (11)}$$

In Eqn. (11, the surface coverage is a function of temperature, which is unknown. Therefore, this equation was further manipulated with the initial condition of $\theta(T = T_i) = \theta_{0,i}$, where T_i is the first temperature point of the TPD spectrum. Surface coverage can then be expressed as followed, with temperature as its only independent variable:

$$\theta_i = \left[\frac{\nu_2 R}{\beta E_d} \cdot T^2 \exp\left(-\frac{E_d}{RT}\right) - \frac{\nu_2 R}{\beta E_d} \cdot T_i^2 \exp\left(-\frac{E_d}{RT_i}\right) + \frac{1}{\theta_{0,i}}\right]^{-1}. \qquad \textbf{Eqn. (12)}$$

Lastly, the values of all $\theta_{0,i}$ with $i = \overline{1..3}$ were calculated based on the proportion of each deconvoluted peak in terms of peak area and θ_0. Figure 23 shows the final simulation of the experiment with β = 38°C/min. This simulation produces a TPD spectrum very close to the experimental data with kinetic parameters obtained from the linear relationship by the compensation effect.

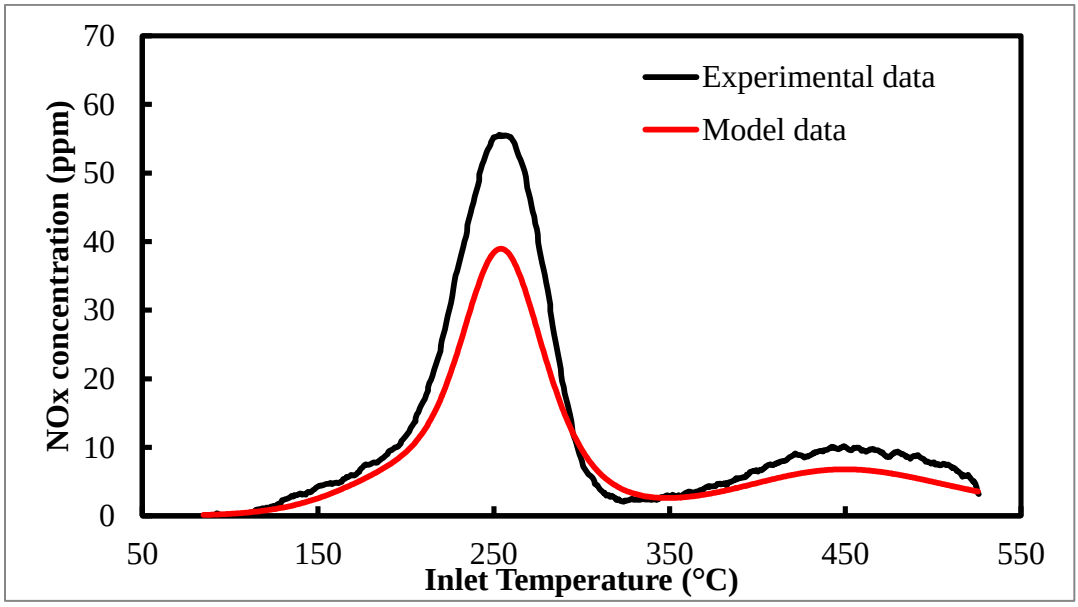

Figure 23 - Full simulation of the TPD profile of the experiment with β = 38°C/min

Figure 24 compares the simulation of peak 2 using kinetic parameters obtained from peak-width analysis vs. Polanyi-Wigner heating rate analysis. It can be seen that the peak-width analysis displays a better fit to experimental data than the latter method.

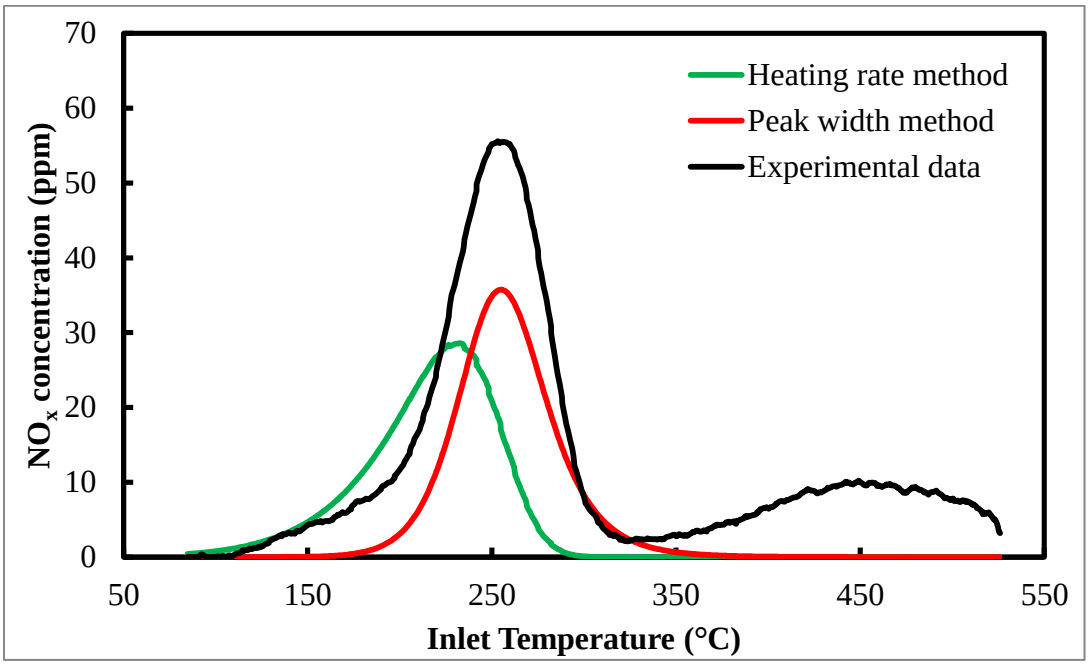

Figure 24 - Peak 2 simulation by heating rate method vs. peak width method of the experiment with β = 38°C/min

5.4 Conclusions

This study attempts to resolve desorption kinetics in the temperature programmed desorption of NO_x on Pd/BEA under the influence of CO and H_2O. Though the combination of heating rate method and Redhead's method can evaluate all important desorption kinetic parameters, its validity is questionable by the underlying assumptions. However, the constraints caused by such assumptions can be overcome by employing the peak width analysis which results in a more reasonable values for the desorption activation energy E_d and the pre-exponential factor ν_n.

The newly obtained desorption kinetic parameters led us to the successful simulations of the experimental TPD spectra. Though it could predict the shape of thermal desorption profiles, the Polanyi-Wigner model did only reveal the desorption kinetics of NO_x activity on Pd/BEA under the influence of O_2, CO, and H_2O but not the actual events at surface level. Though more rigorous approach may be required in terms of elementary reaction steps, these results have brought us closer to fully understanding the remarkable NO storage capacity of Pd/BEA zeolite and the development of an ideal passive NO_x adsorber.

Chapter 6 – Conclusions and Future Plan

This thesis contributes to the understanding of passive NO_x adsorbers, which is helpful for the development of an ideal PNA catalyst in the future. The activity of Pd/BEA PNA was investigated by analysis of TPD and DRIFTS experiments as well as kinetic study from the TPD spectra.

6.1 Conclusions

6.1.1 Effect of CO on Pd/BEA Passive NO_x Adsorbers

NO_x-TPD data show that the addition of CO resulted in increased NO_x uptake at low temperature and induced desorption at higher temperatures. Moreover, DRIFTS experiments showed that Pd at lower oxidation states can bond NO_x more strongly via the strengthening of the covalent bond by π-back-donation from Pd as the metal gains more electrons.

6.1.2 Effect of SO_2 on Pd/BEA Passive NO_x Adsorbers

Through TPD data, SO_2 was shown to hinder NO_x activity to a small extent, but overall it did not significantly alter the uptake or release of NO_x on Pd/BEA passive NO_x adsorber.

6.1.3 Desorption Kinetics of NO_x on Pd/BEA – Effect of Heating Rate

Desorption kinetics of NO_x on Pd/BEA under the influence of CO and H_2O was studied. Kinetic parameters were obtained and cross-verified via heating rate method, Redhead's method, and peak width analysis. The last method eventually produced the most plausible kinetics in terms of fitting experimental data. Parameters calculated from peak width analysis were used to simulate the experimental TPD spectra. The

simulation could predict the peak temperature locations correctly but could not fit the data in terms of peak amplitudes. Interestingly, the frequency factors and activation energies of desorption show compensation effect, which established a linear relationship between $\ln \nu_n$ and E_d. This relationship allows for prediction of desorption kinetic parameters of TPD with heating rates within the scope of this study. However, surface events were left untouched and thus require a more rigorous approach that formally considers the coverage-dependency of the parameters to achieve full understanding of the NO_x low-temperature performance of Pd/BEA zeolite.

6.2 Recommendations for future work

The following recommendations can be carried out to gain more insights into the understanding of Pd/BEA PNA:

i. DRIFTS data reported in this study were obtained in the absence of water. Experiments with water have been done but IR spectral analysis still remains very complicated. Complete understanding of all IR features formed upon water adsorption on Pd/BEA will contribute to the surface changes induced by water. This is critical as for explaining the beneficial effect of water on NO_x storage capacity according to unreported results.

ii. This study disregards the effect of hydrocarbons which are always present in the engine exhaust. Experiments were also done with various concentrations of C_3H_6 in the feed flow, but data were not reported in this thesis. Well-known for its reducing potential, C_3H_6 also showed similar effects as did CO, but at lesser intensity in terms of NO_x storage and release enhancements. However, the analysis was further complicated due to the oxidation of C_3H_6 at higher

temperature. DRIFTS experiments will play an important role in understanding the influence of C_3H_6 in particular and HCs in general to NO_x activity on Pd/BEA PNA. Experiments such as simple adsorption of C_3H_6, co-adsorption of C_3H_6 and NO, co-adsorption of C_3H_6, NO, and CO, with or without water, on hydrothermally aged Pd/BEA will be a good starting point.

iii. Though SO_2 did not show significant effect on NO_x performance, its influence needs further investigation to guarantee that SO_2 will have bearable damage to Pd/BEA PNA. DRIFTS can be used to study how SO_2 interacts with Pd/BEA to elaborate the slight decrease in NO_x uptake and release on this catalyst. Again, the presence of water is also critical in this situation.

iv. The viability and stability of Pd/BEA was not addressed in this study. For this purpose, cycling experiments can be conducted where Pd/BEA is exposed to feed gases the closely resemble diesel exhaust and where the inlet temperature will cycle in between 80°C and 350°C (typical exhaust temperature) with controlled heating and cooling rates. The storage capacity and desorption efficiency over each cycle will be used to measure the sustainability of Pd/BEA performance.

v. The scope of this thesis is limited to Pd/BEA. Other zeolite support materials, such as MFI and CHA, also need to be investigated in the same manner to achieve a more comprehensive understanding of metal-zeolite catalysts. Addition of other metals can also be considered.

References

[1] W.S. Epling, L.E. Campbell, A. Yezerets, N.W. Currier, J.E.I. Parks, "Overview Of The Fundamental Reactions and Degradation Mechanisms Of NO_x Storage/reduction Catalysts," *Catal. Rev. Sci. Eng.* 46 (2004) 163–245. doi:10.1081/CR-200031932.

[2] R.M. Heck, R.J. Farrauto, S.T. Gulati, Catalytic Air Pollution Control: Commercial Technology, John Wiley & Sons, 2009.

[3] M. Gumus, "Reducing Cold-start Emission From Internal Combustion Engines By Means Of Thermal Energy Storage System," *Appl. Therm. Eng.* 29 (2009) 652–660. doi:10.1016/j.applthermaleng.2008.03.044.

[4] K. Ramanathan, D.H. West, V. Balakotaiah, "Optimal Design Of Catalytic Converters For Minimizing Cold-start Emissions," *Catal. Today*. 98 (2004) 357–373. doi:10.1016/j.cattod.2004.08.003.

[5] M.S. Reiter, K.M. Kockelman, "The Problem Of Cold Starts: A Closer Look At Mobile Source Emission Levels," *Ransportation Res. Part D Transp. Environ.* 43 (2016) 123–132.

[6] A.M. Beale, F. Gao, I. Lezcano-Gonzalez, C.H.F. Peden, J. Szanyi, "Recent Advances In Automotive Catalysis For NO_x Emission Control By Small-pore Microporous Materials," *Chem. Soc. Rev.* 44 (2015) 7371–7405. doi:10.1039/C5CS00108K.

[7] L. Lietti, I. Nova, P. Forzatti, "Selective Catalytic Reduction (SCR) Of NO By NH_3 Over TiO_2-supported V_2O_5–WO_3 And V_2O_5–MoO_3 Catalysts," *Top. Catal.* 11/12 (2000) 111–122. doi:10.1023/A:1027217612947.

[8] J. Li, H. Chang, L. Ma, J. Hao, R.T. Yang, "Low-temperature Selective Catalytic Reduction Of NO_x With NH_3 Over Metal Oxide And Zeolite Catalysts—A Review," *Catal. Today*. 175 (2011) 147–156. doi:10.1016/j.cattod.2011.03.034.

[9] Weizhu An, Qinglin Zhang, * and Karl T. Chuang, A.R. Sanger, "A Hydrophobic Pt/Fluorinated Carbon Catalyst For Reaction Of NO With NH_3," (2001). doi:10.1021/IE0104969.

[10] S.L. Suib, Z. Sobalik, "Abatement Of NO_x And N_2O Using Zeolite Catalysts," in: New and Future Developments in Catalysis, 2013: pp. 155–194. doi:10.1016/B978-0-444-53870-3.00007-1.

[11] K. Rahkamaa-Tolonen, T. Maunula, M. Lomma, M. Huuhtanen, R.L. Keiski, "The Effect Of NO_2 On The Activity Of Fresh And Aged Zeolite Catalysts In The NH_3-SCR Reaction," *Catal. Today*. 100 (2005) 217–222. doi:10.1016/j.cattod.2004.09.056.

[12] Z. Liu, P.J. Millington, J.E. Bailie, R.R. Rajaram, J.A. Anderson, "A Comparative Study Of The Role Of The Support On The Behaviour Of Iron Based Ammonia SCR Catalysts," *Microporous Mesoporous Mater.* 104 (2007) 159–170. doi:10.1016/j.micromeso.2007.01.027.

[13] A. Grossale, E. Tronconi, "Study Of A Fe–zeolite-based System As NH_3-SCR Catalyst For Diesel Exhaust Aftertreatment," *Catal. Today*. 136 (2008) 18–27. doi:10.1016/j.cattod.2007.10.117.

[14] F. Gao, Y. Wang, M. Kollár, N.M. Washton, J. Szanyi, C.H.F. Peden, "A Comparative Kinetics Study Between Cu/SSZ-13 And Fe/SSZ-13 SCR Catalysts," *Catal. Today*. 258 (2015) 347–358. doi:10.1016/j.cattod.2015.01.025.

[15] Y. Zheng, M. Li, M. Harold, D. Luss, "Enhanced Low-Temperature NO_x Conversion By High-Frequency Hydrocarbon Pulsing On A Dual Layer LNT-SCR Catalyst," *SAE Int. J. Engines*. 8 (2015) 2015-01–0984. doi:10.4271/2015-01-0984.

[16] J.E. Melville, R.J. Brisley, O. Keane, P.R. Phillips, Mountstevens. Elizabeth Hazel, "Thermally Regenerable Nitric Oxide Adsorbent," 2012. https://patents.google.com/patent/US8105559B2/en (accessed October 18, 2016).

[17] J.A. Cole, "System For Reducing NO_x From Mobile Source Engine Exhaust," 5656244, 1997. https://patents.google.com/patent/US5656244A/en.

[18] Y. Murata, T. Morita, K. Wada, H. Ohno, "NO_x Trap Three-Way Catalyst (N-TWC) Concept: TWC With NO_x Adsorption Properties At Low Temperatures For Cold-Start Emission Control," *SAE Int. J. Fuels Lubr.* 8 (2015) 2015-01–1002. doi:10.4271/2015-01-1002.

[19] R.R. Rajaram, H.-Y. Chen, D. Liu, "Passive NO_x Adsorber," US20150158019, 2015. https://patents.google.com/patent/US20150158019A1/en.

[20] H.-Y. Chen, J.E. Collier, D. Liu, L. Mantarosie, D. Durán-Martín, V. Novák, R.R. Rajaram, D. Thompsett, "Low Temperature NO Storage Of Zeolite Supported Pd For Low Temperature Diesel Engine Emission Control," *Catal. Letters*. 146 (2016) 1706–1711. doi:10.1007/s10562-016-1794-6.

[21] M. Jarvis, K.M. Adams, "Method For Converting Exhaust Gases From A Diesel Engine Using Nitrogen Oxide Absorbent," 6182443, 2001. https://patents.google.com/patent/US6182443B1/en.

[22] Y. Ji, S. Bai, M. Crocker, "Al_2O_3-based Passive NO_x Adsorbers For Low

Temperature Applications," *Appl. Catal. B Environ.* 170–171 (2015) 283–292. doi:10.1016/j.apcatb.2015.01.025.

[23] Y. Ryou, J. Lee, H. Lee, C.H. Kim, D.H. Kim, "Low Temperature NO Adsorption Over Hydrothermally Aged Pd/CeO_2 For Cold Start Application," *Catal. Today*. (2017). doi:10.1016/j.cattod.2017.02.025.

[24] Y. Ji, D. Xu, S. Bai, U. Graham, M. Crocker, B. Chen, C. Shi, D. Harris, D. Scapens, J. Darab, "Pt- And Pd-Promoted CeO_2 –ZrO_2 For Passive NO_x Adsorber Applications," *Ind. Eng. Chem. Res.* 56 (2017) 111–125. doi:10.1021/acs.iecr.6b03793.

[25] S. Jones, Y. Ji, M. Crocker, "CeO_2-M2O3 Passive NO_x Adsorbers For Cold Start Applications," (2016). http://cleers.org/workshops/workshop2016/presentations/2016CLEERS_Jones.pdf (accessed October 18, 2016).

[26] K.D. Kempfert, E.Y. Jiang, S. Oas, J. Coffin, "Detectors For Fourier Transform Spectroscopy," Madison, WI, n.d. http://mmrc.caltech.edu/FTIR/Nicolet/Nicolet Tech Notes/DetectorsforFTIR1204.pdf.

[27] J.P. Blitz, "Diffuse Reflectance Spectroscopy," in: F.M. Mirabella (Ed.), Modern Techniques in Applied Molecular Spectroscopy, John Wiley & Sons, Inc., 1998: p. 192.

[28] A. Vu, J. Luo, J. Li, W.S. Epling, "Effects Of CO On Pd/BEA Passive NO_x Adsorbers," *Catal. Letters*. 147 (2017) 745–750. doi:10.1007/s10562-017-1976-x.

[29] M.K. Khair, W.A. Majewski, Diesel Emissions And Their Control, SAE

International, Warrendale, Pa., 2006.

[30] P. Forzatti, I. Nova, E. Tronconi, "New 'Enhanced NH_3 -SCR' Reaction For NO_x Emission Control," *Ind. Eng. Chem. Res.* 49 (2010) 10386–10391. doi:10.1021/ie100600v.

[31] C. Lambert, R. Hammerle, R. McGill, M. Khair, C. Sharp, "Technical Advantages Of Urea SCR For Light-Duty And Heavy-Duty Diesel Vehicle Applications," in: 2004. doi:10.4271/2004-01-1292.

[32] G. Liu, P.-X. Gao, "A Review Of NO_x Storage/reduction Catalysts: Mechanism, Materials And Degradation Studies," *Catal. Sci. Technol.* 1 (2011) 552. doi:10.1039/c1cy00007a.

[33] M. Sharma, M.P. Harold, V. Balakotaiah, "Analysis Of Storage And Reaction Phases Of LNT For Diesel Engine Exhaust Treatment," in: 2005. doi:10.4271/2005-01-3882.

[34] J. Theis, J. Lupescu, J. Ura, R. McCabe, "Lean NO_x Trap System Design For Cost Reduction And Performance Improvement," in: 2006. doi:10.4271/2006-01-1069.

[35] J. Luo, F. Gao, A.M. Karim, P. Xu, N.D. Browning, C.H.F. Peden, "Advantages Of $MgAlO_x$ Over γ-Al_2O_3 As A Support Material For Potassium-Based High-Temperature Lean NO_x Traps," *ACS Catal.* 5 (2015) 4680–4689. doi:10.1021/acscatal.5b00542.

[36] C. Hess, E. Ozensoy, C.W. Yi, D.W. Goodman, "NO Dimer And Dinitrosyl Formation On Pd(111): From Ultra-high-vacuum To Elevated Pressure Conditions," *J. Am. Chem. Soc.* 128 (2006) 2988–2994. doi:10.1021/ja057131q.

[37] H. Tiznado, S. Fuentes, F. Zaera, “Infrared Study Of CO Adsorbed On Pd/Al_2O_3-ZrO_2. Effect Of Zirconia Added By Impregnation,” *Langmuir*. 20 (2004) 10490–10497. doi:10.1021/la049606h.

[38] E. Ozensoy, D. Wayne Goodman, “Vibrational Spectroscopic Studies On CO Adsorption, NO Adsorption CO + NO Reaction On Pd Model Catalysts,” *Phys. Chem. Chem. Phys.* 6 (2004) 3765. doi:10.1039/b402302a.

[39] J. Yu, F. Guo, Y. Wang, J. Zhu, Y. Liu, F. Su, S. Gao, G. Xu, “Sulfur Poisoning Resistant Mesoporous Mn-base Catalyst For Low-temperature SCR Of NO With NH_3,” *Appl. Catal. B Environ.* 95 (2010) 160–168. doi:10.1016/j.apcatb.2009.12.023.

[40] B.Q. Jiang, Z.B. Wu, Y. Liu, S.C. Lee, W.K. Ho, “DRIFT Study Of The SO_2 Effect On Low-Temperature SCR Reaction Over Fe−Mn/TiO_2,” *J. Phys. Chem. C*. 114 (2010) 4961–4965. doi:10.1021/jp907783g.

[41] J.L. Falconer, J.A. Schwarz, “Temperature-Programmed Desorption And Reaction: Applications To Supported Catalysts,” *Catal. Rev.* 25 (1983) 141–227. doi:10.1080/01614948308079666.

[42] A.M. de Jong, J.W. Niemantsverdriet, “Thermal Desorption Analysis: Comparative Test Of Ten Commonly Applied Procedures,” *Surf. Sci.* 233 (1990) 355–365. doi:10.1016/0039-6028(90)90649-S.

[43] J.W. Niemantsverdriet, K. Markert, K. Wandelt, “The Compensation Effect And The Manifestation Of Lateral Interactions In Thermal Desorption Spectroscopy,” *Appl. Surf. Sci.* 31 (1988) 211–219. doi:10.1016/0169-4332(88)90062-1.